JCI The Journal of Clinical Investigation

# Tryptophan metabolites suppress Wnt pathway and promote adverse limb events in CKD patients

Nkiruka V. Arinze, … , Nader Rahimi, Vipul C. Chitalia

*J Clin Invest.* 2021. https://doi.org/10.1172/JCI142260.

Research In-Press Preview Nephrology Vascular biology

## Graphical abstract

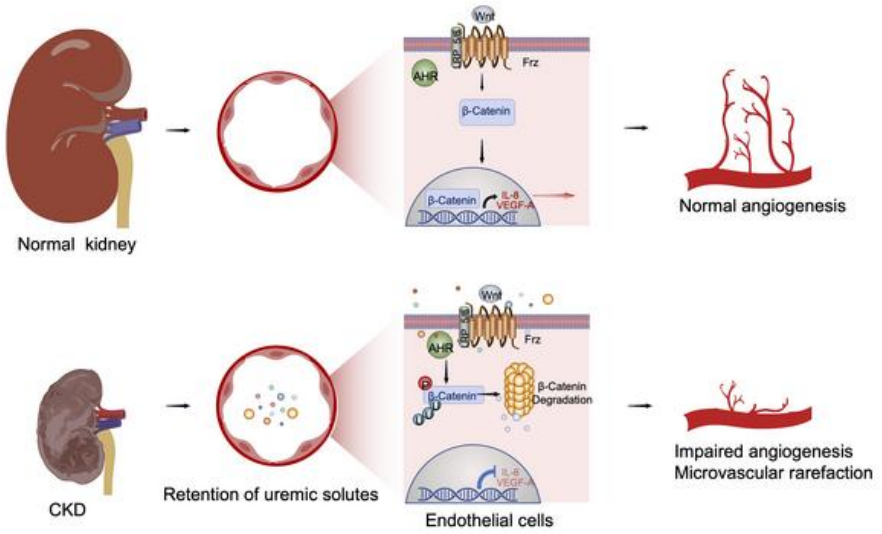

# Tryptophan metabolites suppress Wnt pathway and promote adverse limb events in CKD patients

**Authors:**
Nkiruka V. Arinze[1*], Wenqing Yin[2*], Saran Lotfollahzadeh[2], Marc Arthur Napoleon[2], Sean Richards[2], Joshua A. Walker[2,3], Mostafa Belghasem[4], Jonathan D. Ravid[5], Mohamed Hassan Kamel[2], Stephen A. Whelan[6], Norman Lee[6], Jeffrey J. Siracuse[1], Stephan Anderson[7], Alik Farber[1], David Sherr[8], Jean Francis[2], Naomi Hamburg[3], Nader Rahimi[4], Vipul C. Chitalia[2,9,10#]

* Equal first authorship

**Authors affiliations**:
[1]Division of Vascular and Endovascular Surgery, Department of Surgery, Boston University School of Medicine, Boston, MA 02118, USA
[2]Renal Section, Department of Medicine, Boston University School of Medicine, Boston, MA 02118, USA
[3]Whitaker Cardiovascular Institute, Boston University School of Medicine, Boston, MA 02118, USA
[4]Department of Pathology and Laboratory Medicine, Boston University School of Medicine, Boston, MA 02118, USA
[5]School of Medicine, Boston University School of Medicine, Boston, MA 02118, USA
[6]Chemical Instrumentation Center, Department of Chemistry, Boston University, Boston, MA, 021118, USA
[7]Department of Radiology, Boston University School of Medicine, Boston, MA 02118, USA
[8]Environmental Health Department, School of Public Health, Boston University, Boston, MA 02118, USA
[9]Veterans Affairs Boston Healthcare System, Boston MA 02118, USA
[10] Institute of Medical Engineering and Sciences, Massachusetts Institute of Technology, Cambridge, MA, 02139 USA

# **Corresponding author**:
Vipul Chitalia, M.D., Ph.D.
Renal Section, Department of Medicine, Boston University Medical Center
Evans Biomedical Research Center, X-530
Boston, MA 02118, USA
(P) 617-638-7330, (F) 617-638-7326
Email: vichital@bu.edu

**Keywords**: Angiogenesis, kidney disease, peripheral artery disease, uremic toxins, indoxyl sulfate, Wnt signaling

Total numbers of figures and tables: 7 panels of figures, two tables and 13 panels of supplementary figures and 2 supplementary tables

**COI:** The authors have declared that no conflict of interest exists

**Abstract (199/200 words)**

Chronic kidney disease (CKD) imposes a strong and independent risk for peripheral artery disease (PAD). While solutes retained in CKD patients (uremic solutes) inflict vascular damage, their role in PAD remain elusive. Here, we show that the dietary tryptophan-derived uremic solute including indoxyl sulfate (IS) and Kynurenine (Kyn), at concentrations corresponding to CKD patients suppressed β-catenin in several cell-types including microvascular endothelial cells (EC), inhibiting Wnt activity and proangiogenic Wnt targets in ECs. Mechanistic probing revealed that these uremic solutes downregulated β-catenin, dependent on serine 33 in its degron motif and through Aryl Hydrocarbon Receptor (AHR). Hindlimb ischemia in adenine-induced CKD and IS solute-specific mice models showed diminished β-catenin and VEGF-A in the capillaries and reduced capillary density, which correlated inversely with blood levels of IS and Kyn and AHR activity in ECs. An AHR inhibitor treatment normalized post-ischemic angiogenic response in CKD mice to a non-CKD level. In a prospective cohort of PAD patients, plasma levels of tryptophan metabolites and plasma's AHR-inducing activity in ECs significantly increased the risk of future adverse limb events. This work uncovers tryptophan metabolites-AHR-β-catenin axis as a mediator of microvascular rarefaction in CKD patients and demonstrates its targetability for PAD in CKD models.

.

## Introduction

Peripheral artery disease (PAD) is a global health problem affecting 200 million adults worldwide (1, 2). Chronic PAD is characterized by limb hypoperfusion caused by arterial occlusive disease. It can be asymptomatic, or can manifest across a spectrum, including intermittent claudication or chronic limb threatening ischemia (CLTI) (3). CLTI is the end-stage of PAD presenting with ischemic rest pain or tissue loss (non-healing wounds and/or gangrene), increasing the risk of limb loss. The therapies for PAD are focused on improving limb perfusion to prevent CLTI.

Compared to the general population, patients with chronic kidney disease (CKD) exhibit several unique aspects of PAD (4). Among 1,091,201 patients, those with CKD showed three times higher prevalence of PAD (32%) compared to the non-CKD patients (9.6%) (5). The overall 5-year limb salvage rate in CLTI patients without CKD was 86% and decreased to 50% in patients with stage 5 CKD (6). Even with adjustments for conventional co-morbidities, CKD increases the amputation risk by 3-fold (4, 7). Although CKD and non-CKD patients experience a comparable level of arterial patency following revascularization, CKD portends a higher risk for clinical failure defined as amputation and ulceration, etc. (4, 8, 9). These studies indicate CKD as a strong and independent risk factor for PAD and its complications and implicate CKD-specific risk mediators in PAD pathogenesis.

CKD is characterized by the retention of a host of solutes called uremic solutes/toxins (10). A group of uremic solutes are derived from dietary tryptophan (Trp) and includes indoxyl sulfate (IS), Kynurenine (Kyn) and Kynurenic acid (KA), etc (11). These are known vasculotoxins (12, 13), whose levels increase in the early stages of CKD and rise relentlessly with CKD progression and are not effectively dialyzed (10). The influence of uremia (a biological state induced by CKD) and, these Trp-based uremic toxins, on PAD remain poorly explored.

The pathophysiological response to limb ischemia is complex with a singular goal of compensatory increase in blood flow with the development of macro- and microvasculature (post-ischemic angiogenesis). This is a dynamic process orchestrated by different signaling processes, of which the Wnt pathway is critical (14). The binding of Wnt ligands such as Wnt3a to Wnt receptors initiates a cascade of events such as inhibition of the glycogen synthetase kinase (GSK-3β) culminating upregulation and in nuclear translocation of β-catenin (active β-catenin), the central mediator of Wnt signaling (Wnt-on phase) (15). This event induces pro-proliferative and angiogenic targets, such as Cyclin D1, VEGF-A and IL-8 in endothelial cells (ECs) to increase their proliferation and migration, key processes for angiogenesis. In the absence of a ligand, Wnt signaling is suppressed (Wnt-off phase). Given the central role of Wnt signaling in angiogenesis, we posited that the uremic milieu and Trp-based uremic solutes may downregulate Wnt/β-catenin pathway in ECs and post-ischemic angiogenesis.

## Results

### *Uremic serum suppresses endothelial functions critical for angiogenesis*

We examined the effect of uremia on functions of human dermal microvascular endothelial cells (ECs). The ECs were treated with the pooled sera from twenty end-stage kidney disease (ESKD) patients on hemodialysis (uremic serum). The pooled sera were used first to examine the class effect of CKD. Control sera consisted of age-, sex- and ethnicity-matched controls without CKD (**Supplemental Table 1**). ESKD patients showed no differences in the age, sex, ethnicity and blood pressure compared to controls. However, the groups differed in other comorbidities (**Supplemental Table 1**).

The ECs exposed to uremic serum (final concentration of 5%) showed 30% reduced survival ($p < 0.001$) (**Supplemental Figure 1A**) and a 3-fold lower proliferation ($p < 0.001$) compared to control serum (**Supplemental Figure 1B**). A scratch assay for EC migration showed that ECs exposed to uremic serum migrated half the distance compared to controls ($p = 0.016$) (**Supplemental Figure 1C-1D**).

### *Uremic serum suppresses pro-angiogenic Wnt/β-catenin axis*

The above results suggested that uremic serum suppressed EC functions important in angiogenesis. Wnt/β-catenin signaling is critical for EC survival, proliferation and migration etc. (14). We posited that the uremic serum might suppress Wnt/β-catenin activity in ECs. ECs treated with uremic sera showed a significant reduction in total β-catenin and active β-catenin compared to controls (both $p < 0.001$) (**Figure 1A and Supplemental Figure S1E).** We assessed Wnt activity in ECs expressing β-catenin-responsive promoter tethered to luciferase reporter construct (LS). The luciferase values were normalized to the protein concentration (relative luciferase unit - RLU) (16, 17). β-catenin-unresponsive promoter construct (FuLS) served as a control and showed minimal Wnt activity (**Supplemental Figure 1F**). Uremic serum suppressed Wnt activity in ECs

by > 10-fold compared to controls. IL-8 and VEGF-A, known Wnt targets in ECs (16, 17), showed 50% reduction in the secreted IL-8 ($p = 0.004$) and VEGF-A ($p = 0.009$) compared to controls (**Supplemental Figure 1G and 1H**). Uremic serum reduced Cyclin D1, a pro-proliferative Wnt target induced by Wnt3a ($p = 0.005$) (**Supplemental Figure 1I and J**), as well as *AXIN2* and *MYC* (**Supplemental Figure 1K**).

We further probed the factors that may contribute to Wnt suppressive effect of uremic serum. Wnt activity in target cells is largely modulated by Wnt ligands, which are glycoproteins (18). We evaluated their involvement using heat-inactivated sera, which is likely to denature proteins. Uremic serum suppressed nuclear β-catenin and this effect persisted with the heat-inactivated uremic serum (**Supplemental Figure 1L and 1M**) raising a possibility of non-protein modulators in uremic sera.

***Uremic solutes and Wnt/β-catenin in endothelial cells***

CKD patients retain a host of solutes (non-protein). Water-soluble solutes such as urea (19.98 mM), creatinine (530 μM), oxalic acid (55.53 μM), and homocysteine (19.97 μM) at the concentrations in CKD patients had no effect on β-catenin (**Figure 1B and Supplemental Figure 1N**). In contrast, control sera spiked with IS corresponding to different stages of CKD (**Supplemental Table 2)** emulated the Wnt suppressive effect of uremic serum. IS downregulated cytosolic β-catenin by 22-30% ($p= 0.052$) and nuclear β-catenin to a greater extent (more than 60%, $p < 0.001$) (**Figure 1C**). In both the fractions, compared to control (IS= 0 μM), IS-treated cells showed ~70-80% suppression of β-catenin even at concentrations corresponding to the early stages of CKD (**Figure 1D**, compared to IS = 0 μM, $p = 0.004$ for IS = 5 μM, $p <0.001$ for IS = 10, 50 and 100 μM for both the fractions).

We further confirmed these findings on Wnt activity and using immunofluorescence (IF) assays. ECs were pre-treated with Wnt3a (Wnt-on phase) or vehicle (Wnt-off phase) along with IS (**Figure 1E-1F**). IS suppressed Wnt activity in a dose-dependent manner (Wnt-off phase - $R^2$ 0.542 and $p < 0.001$; Wnt-on phase- $R^2$ 0.768 and $p < 0.001$).

The effect of IS on nuclear β-catenin was analyzed in IF assay using profile plots. Profile plot examines the pixel intensity (Y-axis) throughout the length of cells in microns (X-axis) (**Figure 1G).** IS reduced total β-catenin in ECs by ~ 10-fold (note the differences in the Y-axis scale of Wnt3a- and vehicle-treated cells). The effect on nuclear β-catenin was quantified in randomly selected ECs. Their nuclei were delineated as regions of interest and normalized to the surface area of ECs. This value is presented as the integrated density. Integrated density is a composite of pixel number and intensity and is calculated for the area (micron$^2$), as done previously (19, 20). Wnt3a increased nuclear β-catenin by an 8-10-fold, which was suppressed by IS (**Figure 1H,** compared to vehicle group, Wnt3a **** $p < 0.001$; and compared to Wnt3a, IS+Wnt-3a group *** $p = 0.003$). Collectively these results suggested that IS downregulated Wnt/β-catenin in ECs.

We assessed whether this effect of IS was EC-specific or observed in other cells. In fibroblasts (NIH 3T3) and epithelial cells (human kidney HK-2), IS at 10 μM showed a trend towards increase in cytosolic β-catenin in these cells. However, nuclear β-catenin was consistently downregulated by IS (**Supplemental Figure 2A-2D)**. Skeletal muscle cells were examined due to their involvement in PAD. Treatment of primary human skeletal muscle cells showed that IS monotonically downregulated β-catenin in skeletal muscle cells (**Supplemental Figure 2E-2F)**. These results underscore a broad effect of IS in cell types relevant to PAD.

PAD is characterized by hypoxic environment in the limb. Therefore, we examined the IS-mediated β-catenin regulation under hypoxic environment. ECs exposed to control human serum

spiked with different IS concentrations were grown overnight in a hypoxia chamber with 1% O2. ECs exposed to 21% O2 (normoxia) served as controls. As anticipated, in control samples IS = 0 μM, nuclear β-catenin levels were higher in hypoxia compared to normoxia (21) (**Supplemental Figure 3A and 3B**). Under hypoxia, 1-10 μM IS suppressed nuclear β-catenin to a greater extent than normoxia suggesting more prominent effect of IS on ECs in hypoxic environment. These differences were non-significant at higher concentrations of IS.

***Uremic serum and solutes augment β-catenin ubiquitination and degradation***

IS-induced β-catenin downregulation can be at the transcriptional or post-transcription level. ECs treated with IS showed no changes in *β-catenin* mRNA (**Figure 2A**), suggesting post-transcriptional β-catenin regulation. β-catenin is tightly regulated by proteasomal degradation (15), which was examined by a half-life assay. The translation was blocked with cycloheximide and the amount of time taken for a protein to drop to 50% of its original level was considered its half-life. IS significantly shortened the half-life of β-catenin (Control: 7.6 $\pm$ 0.32 hours, IS: 2.39 $\pm$ 0.46 hours) (**Figure 2B-2C)**. We posited that IS may enhance β-catenin polyubiquitination, which was examined by treating cells with MG138, a proteasome inhibitor. β-catenin ubiquitination was augmented in IS-treated ECs (**Figure 2D-2E**). ECs treated with increasing concentrations of uremic serum (**Figure 2F-2G)** showed increased β-catenin ubiquitination by a 3-4-fold compared to controls ($p < 0.001$). These data suggested that IS and uremic serum augmented β-catenin ubiquitination and degradation in ECs.

***IS regulates β-catenin degradation dependent on serine 33 in the degron motif***

β-catenin N terminus contains a 'degron' motif which regulates its protein stability. This motif is characterized by a series of serine and threonine, which in Wnt-off phase undergo sequential phosphorylation by Casine kinases (CK1 and CKD2) and Glycogen Synthase Kinase

(GSK)-3β (**Figure 3A**) (22). The phosphorylation of serine 33 signals ubiquitinates of flanking lysine residues degrading β-catenin (15). Wnt activation (Wnt-on phase) suppresses GSK-3β and β-catenin undergoes nuclear translocation. We investigated the IS-induced β-catenin regulation by generating a truncation of β-catenin lacking the degron motif (delN- lacking the N terminus of β-catenin) or by introducing a point mutation at serine 33 (S33A) that renders β-catenin stable and transcriptionally active. Also, truncation of C terminus (delC) was created with the intact degron motif (**Figure 3A**).

ECs expressing these Myc-tagged constructs (**Supplemental Figure 4A**) were treated with IS. IS suppressed wild-type and delC β-catenin, while β-catenin S33A and delN remained resistant to IS (**Figure 3B-3C and Supplemental Figure 4B**). This effect of IS corroborated with the IF and half-life studies. Wild-type β-catenin expressed in predominantly in the nuclei was downregulated by IS **(Supplemental Figure 4C**). β-catenin S33A was expressed in the cytosol and nuclei of ECs and showed no changes with IS. Myc-tagged wild-type β-catenin reached 50% of its original level by 8 hours, which was shortened to 4 hours by IS. The half-life of β-catenin S33A was unaltered by IS (**Figures 3 D and E, and Supplemental Figure 4D**). IS increased the polyubiquitination of wild-type β-catenin by a 2-fold (**Figure 3F and Supplemental Figure 5A**), but not of S33A β-catenin. These results suggested that IS augmented β-catenin degradation dependent on serine 33 in the degron motif.

We next examined the effects of IS on Wnt activity and Wnt targets in response to these constructs. Wild-type or S33A β-catenin increased Wnt activity above baseline (**Figure 3G,** β-catenin wild-type or S33A increased Wnt activity from DMSO control # <0.0001; in the IS-treated group, compared to IS = 0 μM, * p = 0.043 and ** p = 0.003). IS suppressed Wnt activity and secreted IL-8 and VEGF-A in ECs media expressing wild-type β-catenin but not β-catenin S33A

(**Supplemental Figure 5B and 5C** marked by #). Lastly, we posited that β-catenin S33A is likely to rescue the IS-mediated Wnt suppression. ECs expressing LS constructs and Flag-tagged wild-type β-catenin were co-transfected with increasing amounts of S33A β-catenin (**Figure 3H and Supplemental Figure 5E**). IS significantly suppressed Wnt activity induced by wild type β-catenin (marked by # in **Figure 3H)**. In WT-transfected cells, compared to control (marked as DMSO), IS suppressed Wnt activity # $p = 0.001$. A combination of 0.4 μg of S33A along with β-catenin WT activity increased Wnt activity compared with β-catenin WT alone ** $p = 0.002$. No difference in Wnt activity was noted between β-catenin WT with DMSO and 0.4 μg of S33A + β-catenin WT treated with IS suggesting that β-catenin S33A restored the Wnt activity to baseline in IS-treated ECs. The levels of IL-8 and VEGF-A followed the Wnt activity (**Supplemental Figure 5D**).

***A set of Trp metabolites regulate Wnt/β-catenin signaling***

We examined whether this effect of IS is shared by other Trp metabolites that are retained in CKD patients (**Supplemental Table 2**). Dietary Trp is processed by the gut microbiome to indole, which is subsequently converted to IS and indole-3 acetic acid **(IA)** in liver. Trp absorbed from gut is converted to Kyn, Anthranilic acid (**AA)**, Kynurenic acid (**KA**), Xanthurenic acid (**XA**) and Quinolinic acid (**QA**) (**Supplemental Figure 6**). They are elevated in patients since early stages of CKD, but their levels vary in patients at the same stage of CKD (23-26) (**Supplemental Table 2**) because their levels are influenced by dietary intake of Trp and processing by intestinal microbiome, etc. ECs expressing LS were exposed to these solutes at concentrations observed in CKD patients in absence (Wnt-off phase) or in presence of lithium chloride, a known inhibitor of GSK3β and Wnt activator (Wnt-on phase) (27, 28) **(Supplemental Figure 7A).** Lithium Chloride significantly upregulated Wnt signaling. Kyn, KA and XA significantly inhibited Wnt activity in

a dose-dependent manner **(Supplemental Figure 7B-7H)**. AA or QA had no effect on Wnt activity in Wnt-on phase. We confirmed the effect of Kyn on β-catenin. ECs treated with Kyn corresponding to different stages of CKD (**Supplemental Table 2**) significantly suppressed nuclear β-catenin (**Supplemental Figure 8A and 8B**) and augmented β-catenin ubiquitination even at concentrations observed in early stages of CKD (**Figure S8C-S8D**). These data suggested that several Trp metabolites suppressed Wnt/β-catenin activity in ECs pointing to a common mechanism of Wnt/β-catenin suppression.

***Uremic serum and solutes suppress Wnt/β-catenin signaling through AHR***

IS, Kyn, KA and XA are activators of Aryl Hydrocarbon Receptor (AHR) pathway in various cells (12, 23, 24, 29). Therefore, we posited that uremic serum and these Trp metabolites regulated Wnt/β-catenin signaling through AHR, which was examined using its genomic and pharmacological manipulation.

We examined mesenchymal embryonic fibroblasts (MEFs) from AHR knock-out (KO) mice and compared them to MEFs with restored AHR expression (knock-in KI cells) (24) (**Figure 4A-4B**). Uremic serum induced ~ 80% downregulation of nuclear β-catenin in the AHR KI MEFs, ($p < 0.001$) compared to controls. While AHR KO MEFs showed a non-significant trend towards reduction in nuclear β-catenin with uremic serum. Importantly, a ~ 2.4-fold reduction in nuclear β-catenin (## $p = 0.032$, **Figure 4B**) was observed with uremic serum-treated AHR KI MEFs compared to AHR KO MEFs. These findings were validated in ECs using AHR CRISPR technique (**Supplemental Figure 9A**), which resulted in substantial downregulation of AHR protein compared to control ECs (**Supplemental Figure 9B**). AHR CRISPR ECs showed ~ 35-55% increase in β-catenin in compared to controls cells ($p <0.001$) (**Supplemental Figure 9C-9D**). The uremic serum-treated control cells showed 60-70% downregulation of β-catenin compared to the

control serum-treated cells (## p = 0.006). This effect of uremic serum was abrogated in AHR CRISPR cells (**Supplemental Figure 9E-9F)**. Uremic serum-treated AHR CRISPR ECs showed ~ a 3.2-fold increase in β-catenin levels compared to control ECs (***p = 0.003). A similar pattern was observed in AHR CRISPR ECs with IS (**Figure 4C)**. IS downregulated β-catenin, which was abrogated in AHR CRISPR ECs **(Figure 4D,** compared to control cells, AHR CRISPR cells ** p = 0.037 for IS = 1 μM and ### p < 0.001 for 10 μM). These results suggested that AHR activity in ECs is necessary for IS- and uremic serum-induced Wnt/β-catenin suppression.

CH223191, a specific AHR inhibitor (24) abrogated β-catenin suppression with uremic serum **(Figure 4E)**. Uremic serum suppressed β-catenin (**Figure 4F,** *** p < 0.001). Compared to uremic-treated control cells, ECs treated with uremic serum+20 μM CH223191 showed a 2-fold upregulation of β-catenin (** p =0.004). AHR inhibition restored IS-induced suppression of Wnt activity **(Figure 4G)**. IS suppressed Wnt activity in the presence of Wnt3a or vehicle. However, cotreatment of IS + 20 μM CH223191 upregulated the Wnt activity (compared to ECs-treated with Wnt3a + IS, those with Wnt3a + IS+ CH223191 increased Wnt activity *** p = 0.01, ## p = 0.041). A similar increase in Wnt activity was noted with Kyn in its highest concentration (5 μM, **Figure 4H**). Compared to ECs-treated with Wnt3a + Kyn, those co-treated with Wnt3a + Kyn + CH223191 showed higher Wnt activity *** p = 0.001, * p = 0.025 (**Figure 4H)**.

Lastly, we assessed Wnt activity with increasing concentrations of CH223191. ECs expressing LS construct were treated with 5% pooled uremic serum, which suppressed Wnt activity compared with control serum (noted as # p = 0.01 in **Figure 4I**). Compared to the uremic serum alone, co-treatment of uremic serum + CH223191 increased Wnt activity in ECs (** p = 0.01 at 5 μM, *** p = 0.001 for 10 and 20 μM). In fact, there was no significant (NS, **Figure 4I**) difference in the Wnt activity between control- and uremic+CH223191-treated cells. These results

suggested that AHR inhibitor restored Wnt suppression in the CKD milieu to the level of non-CKD.

***IS reduces vasculogenesis in zebrafish***

We probed the effect of IS in a Fli1-eGFP transgenic zebrafish model, a well-established model of de novo angiogenesis (vasculogenesis). In this model, ECs are genetically engineered to express eGFP (17). The thickness and bifurcation of intersegmental vessel (ISV) and tail microvasculature are biological readouts. Zebrafish embryos observed at 24 hours post-fertilization (hpf) were treated with IS for an additional 48 hours. Zebrafish exposed to IS showed reduced ISV length and thickness and reduced bifurcation of ISVs (white and blue arrowheads, **Supplemental Figure 10A and B**). Compared to DMSO controls, IS at 50 μM suppressed the tail microvasculature by 47% ($p = 0.012$) and by 90% at 100 μM ($p = 0.002$) (**Supplemental Figure 10C and D**). This model demonstrated the suppressive effect of IS on vasculogenesis.

***IS suppressed Wnt/ β-catenin axis in the capillaries and post-ischemic angiogenesis in mice***

Human PAD is induced in responses to arterial occlusion and this pathology is not well emulated in the zebrafish model. We investigated the effect of IS in a hindlimb ischemia (HLI) model, which is a widely used murine model of PAD. Mice exposed to IS (30, 31) underwent HLI (**Figure 5A**). In this model, the mice were administered IS in drinking water and its excretion was suppressed by Probenecid raising blood levels of IS corresponding to advanced CKD patients (30, 31). Mice treated with Probenecid served as controls. The blood urea nitrogen (BUN) of mice were comparable between both the groups, suggesting their normal renal function (**Supplemental Figure 11A**). Serum IS levels were ~ 12-fold higher in IS-administered mice compared to the control ($p < 0.001$) (**Supplemental Figure 11B**). This model examined the effect of higher levels of IS over a short time frame.

The capillary density was examined using CD31, a marker of ECs and normalized to muscles stained with α-Actin (**Figure 5B**). Expression of both these proteins on IF was examined in randomly obtained images of muscles in each mouse and was quantitated as the integrated density, as done previously (19, 20). Compared to the integrated density of CD31/SMA+ for probenecid-exposed controls, a ~ 30% reduction was observed in IS-exposed mice ($p = 0.0014$) (**Figure 5C**).

The β-catenin levels were examined in the lysates of posterior calf muscles from the ligated limbs. The CKD mice showed~ a 1.5-fold lower β-catenin than the controls ($p = 0.034$) (**Figure 5D-5E**). This reduction in β-catenin can be from capillaries and/or skeletal muscles. We observed β-catenin reduction in both the capillaries and skeletal muscles in IS-treated mice compared to control mice (**Figure 5F,** white arrowhead pointing to a capillary and white asterisk to skeletal muscle fibers). We further quantitated reduction in both these cell types. First, a region of interest (ROI) involved the muscle fiber along with the capillaries (**Figure 5F**, blue dotted line) and its integrated density was noted. A similar analysis was performed by delineating muscle alone (**Figure 5F**, white dotted line). The difference between these two values provided the β-catenin levels in capillaries. β-catenin expression in muscle was reduced by 10-12% in IS-treated mice compared to control mice ($p = 0.054$) (**Figure 5F** white asterisk **and 5G**). A greater reduction in β-catenin was observed in capillaries (4-fold) in IS-treated mice compared to the control mice ($p < 0.001$) (**Figure 5F** white arrowhead **and Figure 5G**). VEGF-A expression was exclusively observed in the capillaries, as identified by colocalization with CD31 (**Figure 6A**, white arrowhead). As capillary density is reduced in IS-treated muscles, it can impact the evaluation of VEGF-A expression, and therefore, we normalized VEGF-A expression to CD31. IS-treated muscles showed ~ 50% reduction in normalized VEGF-A expression ($p = 0.001$) (**Figure 6B**).

To further establish the role of IS in post-ischemic angiogenesis, we performed correlation analyses of the serum levels of IS in mice (obtained at the end of the experiment) with the features of post-ischemia angiogenesis. The levels of IS correlated inversely with the capillary density ($R^2$ 0.499, $p < 0.001$), β-catenin levels in the capillaries ($R^2$ 0.405, $p < 0.001$) and VEGF-A expression ($R^2$ 0.518, $p < 0.001$) (**Figure 6C-6E**).

Next, we investigated relationships between AHR and Wnt activities in ECs in response to sera from mice exposed to IS. Sera from mice at a final concentration of 5% were used to treat ECs stably expressing LS construct (Wnt activity) or xenobiotic-responsive element (XRE)-promoter tethered to luciferase reporter (to measure AHR activity). A 3-fold downregulation in EC Wnt activity ($p < 0.001$) and ~ 2-fold upregulation of AHR activity ($p = 0.002$) was observed in response to sera from mice exposed to IS compared to the control group (**Figure 6F-6G**). AHR activity in the ECs negatively correlated with Wnt activity ($R^2$ 0.518, $p < 0.001$) (**Figure 6H**). Importantly, IS levels in the blood of the CKD mice inversely correlated with EC Wnt activity ($R^2$ 0.897, $p < 0.001$) (**Figure 6I)**. These results demonstrated that a short exposure to IS at high levels significantly downregulated β-catenin and VEGF-A expression in capillaries and reduced capillary density.

***CKD milieu suppresses post-ischemic angiogenesis and Wnt/β-catenin axis in capillaries and muscles***

Next, we examined the post-ischemic angiogenesis and role of AHR signaling in a CKD model. We used an adenine-induced CKD mouse model, which is characterized by high blood levels of IS and Kyn (30, 31) and recapitulated several uremic manifestations (30, 32). A group of 10 C57BL/6 mice was exposed to 0.2% adenine diet and underwent HLI on day 4 after adenine diet (**Figure 7A).** Mice on a normal diet served as controls and all of them were followed for a

total of 21 days before the harvest. Kidneys of adenine-exposed mice showed glomerulosclerosis, tubular dilatation, and interstitial fibrosis **(Supplemental Figure 12A**), and had a significant increase in interstitial fibrosis and tubular atrophy (IFTA) score (33) (**Supplemental Figure 12B**). Compared to the control mice, adenine-treated mice showed increases in BUN and creatinine (**Supplemental Figure 12C-12D)** and a 7-fold increase in serum IS levels ($p < 0.001$) (**Supplemental Figure 12E)**.

Capillary perfusion recovery was followed over 21 days using a laser doppler and presented as a ratio of perfusion in the ligated limb to the un-ligated limb (**Figure 7B**). On post-op day 7, the perfusion ratio of mice on adenine diet was half of the control mice on a normal diet ($p = 0.05$) and remained reduced at 14 ($p < 0.001$) and 21-day post-HLI ($p = 0.002$) (**Figure 7C**). Consistent with the above findings, the muscles of ligated limbs of adenine exposed mice showed ~ 50% reduced capillaries ($p < 0.001$) (**Figure 7D-7E**).

The mice on an adenine diet showed 80% reduction in β-catenin protein compared to the control ($p < 0.001$) (**Supplemental Figure 12F-12G**). Our IF studies demonstrated ~ 40% reduction of β-catenin in skeletal muscles and a greater reduction in β-catenin (90%) in capillaries in adenine mice compared to the control mice (**Figure 7F-7G**). Adenine-treated mice showed ~ 80% reduction in capillary VEGF-A expression ($p = 0.006$) (**Figure 8A-8B**). Taken together, CKD mice showed lower β-catenin expression in muscles and capillaries and capillary density, all of which corroborated with poor perfusion recovery in CKD mice.

Our regression analysis revealed that blood levels of IS in mice inversely correlated with the capillary density measured by the ratio of CD31+/SMA+ ($R^2$ 0.40, $p < 0.001$), β-catenin in the capillaries ($R^2$ 0.78, $p < 0.001$) and VEGF-A expression in the capillaries ($R^2$ 0.68, $p < 0.001$) (**Figure 8C-8E**). We correlated AHR and Wnt activity in ECs in response to sera obtained from

CKD mice. Our results showed a 2.5-fold downregulation in EC Wnt activity ($p < 0.001$) and ~ 1.8-fold upregulation of AHR activity ($p = 0.002$) in response to sera from CKD mice (**Supplemental Figure 12 H and 12I**). EC AHR activity negatively correlated with Wnt activity ($R^2$ 0.518, $p < 0.001$) (**Supplemental Figure 12J**). IS levels inversely correlated with EC Wnt activity ($R^2$ 0.897, $p < 0.001$). AHR activity in ECs induced by the sera of CKD mice correlated negatively with the capillary density in such mice ($R^2$ 0.520, $p = 0.018$) (**Figure 8F-8G**). A similar inverse correlation was observed in CKD mice's blood levels of Kyn and their capillary density, normalized β-catenin and VEGF-A expressions in the capillaries of these mice (**Supplemental Figure 13A-13D**). The blood levels of Kyn in CKD mice negatively correlated with Wnt activity in ECs (**Supplemental Figure 13E**). All these results strongly suggested that the circulating levels of IS and Kyn in blood and AHR activity induced by their sera suppressed the Wnt signaling in ECs and post-ischemic angiogenesis in CKD mice.

***AHR inhibitor normalizes the post-ischemic angiogenesis in CKD mice to a non-CKD state***

The role of AHR signaling in mediating the above-described effects in CKD mice was examined using AHR inhibitors. A total of 32 mice were initiated on adenine diet (30, 31) or normal diet (N= 16/group) (**Figure 9A**). After 7 days of the diet, the mice underwent HLI and were randomly divided to receive CH223191 (10 mg/kg, N= 8) or vehicle (DMSO, N= 8) once a day by IP injection for 5 days on and 2 days off for 17 days on adenine or normal diet. Seven days of adenine diet resulted in BUN of 47.3 $\pm$ 5.8 mg/dl corresponding to the early-stage CKD. This experimental strategy mimics PAD initiation in humans at the early stages of CKD and its progression with deterioration of renal function (4). At the end of the experiment, mice on an adenine diet showed significantly higher BUN. However, there was no difference in BUN in mice with an adenine diet + CH223191 compared to the vehicle-exposed adenine mice (**Supplemental Figure 14A**).

Compared to the mice on normal diet, the mice treated with normal diet + CH223191 showed an increase in the perfusion ratio at 21 days ($p = 0.012$) and capillary density as measured by normalized CD31+/SMA+ cells ($p = 0.041$). The mice on normal diet + CH223191 also demonstrated an upregulation of capillary β-catenin in the capillaries ~ 30% ($p = 0.026$) and VEGF-A by 27% ($p = 0.053$) and skeletal muscle β-catenin by ~ 50% ($p = 0.006$) (**Supplemental Figure 14B-14E**) compared to control mice.

AHR inhibition improved these post-ischemic angiogenesis parameters to a greater extent in CKD mice. Approximately 50% increase in the perfusion ratio was observed within 7 days of treatment with CH223191 and this pattern continued till the end of the experiment (**Figure 9B**, compared to mice on adenine diet one vehicle, mice on adenine diet + CH223191 **$p = 0.04$ for day 14 and *** $p = 0.001$ in day 21). Notably, an increase in the perfusion ratio in CKD mice treated with CH223191 was comparable to that in mice on a normal diet (non-CKD) (shown as a dotted line **Figure 7B**). Compared to adenine mice treated with vehicle, adenine mice on CH223191 showed a 2-fold increase in capillary density ($p = 0.004$), a 3-fold increase in β-catenin expression in the capillaries ($p = 0.002$), a 2-fold increase in β-catenin expression in skeletal muscles ($p = 0.007$) and approximately a 1.8-fold increase in VEGF-A expression in the capillaries ($p = 0.006$) (**Figure 9C-9F and 10A-10B**). Importantly, there were no differences in these parameters in CKD mice treated with CH223191 compared to mice on normal diet (non-CKD) group (represented as dotted lines in **Figure 9B, 9D, 9F and 10B**). All these data suggested that the AHR inhibitor normalized post-ischemia angiogenesis in CKD mice to a non-CKD level.

We further examined the correlation between EC AHR and Wnt activities induced by-sera from CKD mice with their angiogenic parameters (**Figure 10C-10F**). Sera of CKD mice exposed to CH223191 showed a ~ 2-fold suppression of AHR activity in ECs compared to sera derived

from vehicle-treated adenine mice (**Figure 10C**). Compared to sera from vehicle-treated adenine mice, ECs Wnt activity was 1.8-fold higher in response to sera from mice administered CH223191 (**Figure 10D**). AHR activity in ECs inversely correlated with Wnt activity in ECs ($R^2 = 0.48$, $p = 0.00$)2 (**Figure 10E**). There was a strong and significant inverse correlation between serum induced AHR activity in ECs, and capillary density in the mice from which the serum was derived ($R^2 = 0.39$, $p = 0.030$) (**Figure 10F**). These studies suggested that CH223191 treatment suppressed AHR activity in ECs and upregulated Wnt activity in ECs to improve the post-angiogenic response in muscles of CKD mice.

***Trp metabolite levels correlate with adverse limb outcomes in PAD patients.***

To examine the relevance of our findings to humans, we used two separate cohorts of patients. A cohort of ESKD patients without PAD was probed with the hypothesis that their sera will induce a higher AHR activity and greater suppression of Wnt activity in ECs and that these activity levels will correlate with the levels of Trp metabolites. ECs expressing LS or an XRE-responsive promoter were exposed to individual serum from CKD patients (uremic sera) and compared to sera derived from age-, sex- and ethnic background-matched controls (**Supplemental Table 1**). We had previously reported significantly higher levels of IS in these uremic sera (24). Our expanded analysis showed higher levels of Kyn in them (uremic sera 351 $\pm$ 217 nM vs controls -124.1 $\pm$ 109.9 nM, $p < 0.001$). Exposure of ECs to uremic sera resulted in greater AHR activity ($p < 0.001$) and suppressed Wnt activity ($p = 0.017$) compared to those treated with control sera. EC Wnt activity inversely correlated with the levels of IS ($R^2 = 0.34$, $p < 0.001$) and Kyn ($R^2 = 0.25$, $p = 0.025$) in ESKD patients (Supplemental **Figure 15A and 15B**).

We further sought to determine the relevance of Trp metabolites in the pathogenesis of PAD complications in a clinical sample. We examined a nested case-control study from a cohort of

patients with lower extremity PAD (defined as ABI < 0.9 or history of prior revascularization) who were followed prospectively for 2 years for PAD clinical events. Of the entire cohort of 348 patients, 28 patients who experienced an adverse limb event had adequate remaining plasma samples for metabolite measurement. These patients were matched by age, sex, eGFR to 35 PAD patients without adverse limb events (control group). The PAD patients with metabolite measurements were older but otherwise were like the patients without metabolite measurements. Of the 28 patients with adverse limb events, the events included new or worsening claudication (N=9), critical limb threatening ischemia (N=8), limb loss (N=2), graft or stent thrombosis (N=2), any amputation (N=6), stenosis/restenosis (N=7), and new revascularization procedures (N=8). Patients may have had more than one event, but first event date was used for analysis. The events were adjudicated by a panel of 3 physicians using pre-specified definitions. Plasma samples collected at baseline were stored at -80$^0$C. There were no differences in PAD patients' clinical characteristics of who experienced a limb event compared to those without limb events (**Table 1**).

The plasma of PAD patients who subsequently developed adverse limb events showed higher IS levels (5.8 $\pm$ 5.3 μM) than PAD patients without adverse limb events (3.45 $\pm$ 2.9 μM, p = 0.028). Similarly, Kyn levels were 2.2-fold higher in PAD patients with adverse limit (308.5 $\pm$ 215.1 nM vs controls 141.6 $\pm$ 45.26 nM, p <0.001), KA (PAD with adverse limb event- 776.1 $\pm$ 519.7 nM vs controls -521.6 $\pm$ 302.5 nM, p <0.001) and XA (PAD with adverse limb event- 3.9 $\pm$ 1.9 μM vs controls – 2.61 $\pm$ 0.85 μM, p <0.001). There were no differences in the levels of Trp, AA and QA between the two groups. Notably, the concentrations range of IS and Kyn found in PAD patients with events downregulated Wnt/β-catenin activity in ECs to a greater extent (**Figure 1 and 2 and Supplemental Figure 8B-8D**) compared to those levels seen in PAD patients without event.

The plasma from PAD patients with adverse events activated AHR activity in ECs 60% higher compared to the group without adverse event ($p = 0.017$) and suppressed Wnt activity in ECs to a greater extent, as compared to plasma derived from PAD patients without adverse limb events ($p = 0.032$). A Cox proportional hazard model was developed for the incidence of adverse limb events adjusting for age, sex and eGFR. Higher plasma levels of IS, Kyn, KA, XA and the extent of ECs AHR induction and Wnt suppression by these plasma samples were associated with greater risk of adverse limb events (**Table 2**). In contrast, AA and QA were not associated with adverse limb events. These findings suggested that Trp metabolites with Wnt suppressive effect in ECs (**Supplemental Figure 7**) were higher in PAD patients with adverse limb events and contributed to the risk of adverse limb events in them.

## Discussion

While the general mechanisms of PAD pathogenesis are well delineated, there is a distinct paucity of studies elucidating the risk-specific mediators of PAD. Addressing this knowledge gap in CKD, we demonstrate that a specific set of uremic solutes derived from Trp metabolism downregulates Wnt signaling through the AHR pathway in ECs and post-ischemic angiogenesis and induces capillary rarefaction in CKD mice. These specific Trp metabolites significantly increase the risk of future adverse limb events in PAD patients. This work uncovers a mechanistic link between Trp-derived uremic solutes with PAD and AHR as a potential therapeutic target in PAD in CKD patients.

*Trp metabolites and PAD*

Several Trp metabolites induced a similar cellular effect (Wnt/β-catenin suppression) in different cell types. These observations along with other examples (12, 13, 23, 24, 30) support a 'group' effect of a set of uremic toxins. This phenomenon can be explained by mediation of their effect through AHR and creates an opportunity to target AHR to suppress effects of several toxins simultaneously (34). Endothelial dysfunction is universal in CKD patients and is known to be mediated in part by uremic solutes such as IS (11). The results of the current work raise a possible involvement of Wnt signaling in EC dysfunction in CKD patients. β-catenin plays important roles in skeletal muscle energy metabolism, mitochondrial health and structural integrity (35). Downregulation of β-catenin in CKD mice muscles may explain the sarcopenia in CKD patients (36). There are cell-type specific E3 ligases of β-catenin targeting its specific regions. IS regulating β-catenin through its degron motif points to a specific E3 ligase, which warrants further investigation.

*The translational potential of Trp metabolites-Wnt/β-catenin angiogenesis axis*

These data suggest that IS and Kyn increase the risk of PAD initiation and progression up to complications with renal deterioration, a notion supported in clinical studies (37). Not all CKD patients are at an equal risk for PAD or its complications (6). The current study strongly suggests that CKD stage alone based on creatinine is insufficient to stratify PAD patients and supports studies exploring the biomarker potential of these uremic solutes to stratify CKD patients at risk for PAD and its complications. Interestingly, AHR inhibitor in CKD models normalized the post-ischemic angiogenesis to a non-CKD level, in a manner similar to the uremic thrombosis (30). AHR inhibitors are undergoing clinical trials for other indications (38) and can be repurposed for PAD in CKD.

The adenine mouse model was selected for high IS and Kyn levels and its ability to recapitulate uremic features. However, this model is not characterized by proteinuria, a known risk factor of PAD (4). Post-ischemic angiogenesis is a complex process dynamically orchestrated by several cell types, including immune cells, pericytes and vascular smooth muscle cells, etc. Further work is needed to generate a detailed mechanistic understanding of the effects of uremic toxins on different cell types involved in angiogenesis and skeletal muscles in the context of PAD.

This work provides the first mechanistic link between a group of uremic toxins, Wnt signaling and PAD and paves the way for delineating risk-specific mediators of PAD. This study serves as a foundation for future investigation to examine the predictive power of Trp metabolites for refining the stratification of CKD patients at risk for PAD and explore AHR inhibitors as a therapeutic target for PAD complications.

## Material and methods

### Human subjects

Human subjects, laser doppler analysis, IHC, HLI model, adenine CKD model, IS-specific solute model, cells culture and chemical treatment, generation of AHR CRISPR cell line, subcellular fractionation, Wnt activity, immunoblotting, 3[H] Thymidine incorporation assay, qRT-PCR and ELISAs and zebrafish angiogenesis assays and statistical analysis are described in the supplementary information.

**Study approvals**: Both the human and animal studies were conducted after the approval of the Institutional Review Board at Boston University (IRB, H-26367) and written informed consent and Institutional Animal Care and Use Committee (IACUC, PROTO201800298) and Institutional Biosafety Committee (IBC).

**Acknowledgements**

The authors thank Dr. Reiko Matsui and Marcy Silver (WCVI and Boston University School of Medicine BUSM) for their guidance in the HLI model, Dr. Michael Kirber at the BUMC Imaging Core facility for his assistance in confocal microscopy, Dr. Robert Weisbord (WCVI, BUSM) for providing the samples of PAD patients at Boston Medical Center. We also thank Prof. Howard Cabral, PhD, MPH, Boston University School of Public Health and Department of Biostatistics for statistical insight. A portion of this work was presented at the 2019 annual American Society of Nephrology and American Heart Association meetings.

**Sources of Funding**

This work was funded in part by NIH R01HL132325 and R21 DK119740 (VCC), American Heart Association CAT-HD Center grant # 857078 (VCC and SL); and T32 training grant in cardiovascular biology T32 HL007224-40 (JW); T32 training grant in immunobiology of trauma T32 GM086308-06A1 (NA).

**Authors contributions:** NVA and WY have equal contribution to this work; VCC conceived of the hypothesis; VCC, NR, NVA and WY designed the research; NVA, MB and SL performed the HLI; WY, MAN, SR, SL, JAW and MAN performed the experiments; VCC, MAN and MB performed immunofluorescence studies; JAW, MKH, DS, JDR, JJS, SA, AF and JF provided scientific input and data analyses; AF and NH performed the prospective human study, NH performed the analysis of BMC PAD cohort, VCC performed analysis of in vitro and in vivo studies; VCC, NVA and WY prepared the manuscript; All the authors edited the manuscript.

**Disclosures**

The authors have no conflicts of interest to disclose.

## References:


1. Sampson UK, Fowkes FG, McDermott MM, Criqui MH, Aboyans V, Norman PE, et al. Global and regional burden of death and disability from peripheral artery disease: 21 world regions, 1990 to 2010. *Glob Heart.* 2014;9(1):145-58 e21.
2. Fowkes FG, Aboyans V, Fowkes FJ, McDermott MM, Sampson UK, and Criqui MH. Peripheral artery disease: epidemiology and global perspectives. *Nat Rev Cardiol.* 2017;14(3):156-70.
3. Farber A. Chronic Limb-Threatening Ischemia. *N Engl J Med.* 2018;379(2):171-80.
4. Arinze NV, Gregory A, Francis JM, Farber A, and Chitalia VC. Unique aspects of peripheral artery disease in patients with chronic kidney disease. *Vasc Med.* 2019;24(3):251-60.
5. Foley RN, Murray AM, Li S, Herzog CA, McBean AM, Eggers PW, et al. Chronic kidney disease and the risk for cardiovascular disease, renal replacement, and death in the United States Medicare population, 1998 to 1999. *J Am Soc Nephrol.* 2005;16(2):489-95.
6. Owens CD, Ho KJ, Kim S, Schanzer A, Lin J, Matros E, et al. Refinement of survival prediction in patients undergoing lower extremity bypass surgery: stratification by chronic kidney disease classification. *J Vasc Surg.* 2007;45(5):944-52.
7. O'Hare AM, Glidden DV, Fox CS, and Hsu CY. High prevalence of peripheral arterial disease in persons with renal insufficiency: results from the National Health and Nutrition Examination Survey 1999-2000. *Circulation.* 2004;109(3):320-3.
8. Simons JP, Goodney PP, Nolan BW, Cronenwett JL, Messina LM, Schanzer A, et al. Failure to achieve clinical improvement despite graft patency in patients undergoing infrainguinal lower extremity bypass for critical limb ischemia. *J Vasc Surg.* 2010;51(6):1419-24.
9. Patel VI, Mukhopadhyay S, Guest JM, Conrad MF, Watkins MT, Kwolek CJ, et al. Impact of severe chronic kidney disease on outcomes of infrainguinal peripheral arterial intervention. *J Vasc Surg.* 2014;59(2):368-75.
10. Vanholder R, Schepers E, Pletinck A, Nagler EV, and Glorieux G. The uremic toxicity of indoxyl sulfate and p-cresyl sulfate: a systematic review. *J Am Soc Nephrol.* 2014;25(9):1897-907.
11. Ravid JD, and Chitalia VC. Molecular Mechanisms Underlying the Cardiovascular Toxicity of Specific Uremic Solutes. *Cells.* 2020;9(9).
12. Gondouin B, Cerini C, Dou L, Sallee M, Duval-Sabatier A, Pletinck A, et al. Indolic uremic solutes increase tissue factor production in endothelial cells by the aryl hydrocarbon receptor pathway. *Kidney Int.* 2013;84(4):733-44.
13. Chitalia VC, Shivanna S, Martorell J, Balcells M, Bosch I, Kolandaivelu K, et al. Uremic serum and solutes increase post-vascular interventional thrombotic risk through altered stability of smooth muscle cell tissue factor. *Circulation.* 2013;127(3):365-76.
14. Goodwin AM, and D'Amore PA. Wnt signaling in the vasculature. *Angiogenesis.* 2002;5(1-2):1-9.
15. Nusse R. Wnt signaling in disease and in development. *Cell Res.* 2005;15(1):28-32.
16. Chitalia V, Shivanna S, Martorell J, Meyer R, Edelman E, and Rahimi N. c-Cbl, a ubiquitin E3 ligase that targets active beta-catenin: a novel layer of Wnt signaling regulation. *J Biol Chem.* 2013;288(32):23505-17.
17. Shivanna S, Harrold I, Shashar M, Meyer R, Kiang C, Francis J, et al. The c-Cbl ubiquitin ligase regulates nuclear beta-catenin and angiogenesis by its tyrosine phosphorylation mediated through the Wnt signaling pathway. *J Biol Chem.* 2015;290(20):12537-46.
18. Dejana E. The role of wnt signaling in physiological and pathological angiogenesis. *Circ Res.* 2010;107(8):943-52.
19. Belghasem M, Roth D, Richards S, Napolene MA, Walker J, Yin W, et al. Metabolites in a mouse cancer model enhance venous thrombogenicity through the aryl hydrocarbon receptor-tissue factor axis. *Blood.* 2019;134(26):2399-413.

20. Lyle C, Richards S, Yasuda K, Napoleon MA, Walker J, Arinze N, et al. c-Cbl targets PD-1 in immune cells for proteasomal degradation and modulates colorectal tumor growth. *Sci Rep.* 2019;9(1):20257.
21. Xu W, Zhou W, Cheng M, Wang J, Liu Z, He S, et al. Hypoxia activates Wnt/beta-catenin signaling by regulating the expression of BCL9 in human hepatocellular carcinoma. *Sci Rep.* 2017;7:40446.
22. Guharoy M, Bhowmick P, Sallam M, and Tompa P. Tripartite degrons confer diversity and specificity on regulated protein degradation in the ubiquitin-proteasome system. *Nat Commun.* 2016;7:10239.
23. Kolachalama VB, Shashar M, Alousi F, Shivanna S, Rijal K, Belghasem ME, et al. Uremic Solute-Aryl Hydrocarbon Receptor-Tissue Factor Axis Associates with Thrombosis after Vascular Injury in Humans. *J Am Soc Nephrol.* 2018;29(3):1063-72.
24. Shivanna S, Kolandaivelu K, Shashar M, Belghasim M, Al-Rabadi L, Balcells M, et al. The Aryl Hydrocarbon Receptor is a Critical Regulator of Tissue Factor Stability and an Antithrombotic Target in Uremia. *J Am Soc Nephrol.* 2016;27(1):189-201.
25. Barreto FC, Barreto DV, Liabeuf S, Meert N, Glorieux G, Temmar M, et al. Serum indoxyl sulfate is associated with vascular disease and mortality in chronic kidney disease patients. *Clin J Am Soc Nephrol.* 2009;4(10):1551-8.
26. Debnath S, Velagapudi C, Redus L, Thameem F, Kasinath B, Hura CE, et al. Tryptophan Metabolism in Patients With Chronic Kidney Disease Secondary to Type 2 Diabetes: Relationship to Inflammatory Markers. *Int J Tryptophan Res.* 2017;10:1178646917694600.
27. Chitalia VC, Foy RL, Bachschmid MM, Zeng L, Panchenko MV, Zhou MI, et al. Jade-1 inhibits Wnt signalling by ubiquitylating beta-catenin and mediates Wnt pathway inhibition by pVHL. *Nat Cell Biol.* 2008;10(10):1208-16.
28. Cohen P, and Frame S. The renaissance of GSK3. *Nature reviews Molecular cell biology.* 2001;2(10):769-76.
29. Schroeder JC, Dinatale BC, Murray IA, Flaveny CA, Liu Q, Laurenzana EM, et al. The uremic toxin 3-indoxyl sulfate is a potent endogenous agonist for the human aryl hydrocarbon receptor. *Biochemistry.* 2010;49(2):393-400.
30. Shashar M, Belghasem ME, Matsuura S, Walker J, Richards S, Alousi F, et al. Targeting STUB1-tissue factor axis normalizes hyperthrombotic uremic phenotype without increasing bleeding risk. *Sci Transl Med.* 2017;9(417):1-11.
31. Walker JA, Richards S, Belghasem ME, Arinze N, Yoo SB, Tashjian JY, et al. Temporal and tissue-specific activation of aryl hydrocarbon receptor in discrete mouse models of kidney disease. *Kidney Int.* 2020;97(3):538-50.
32. Jia T, Olauson H, Lindberg K, Amin R, Edvardsson K, Lindholm B, et al. A novel model of adenine-induced tubulointerstitial nephropathy in mice. *BMC Nephrol.* 2013;14:116.
33. Belghasem ME, A'Amar O, Roth D, Walker J, Arinze N, Richards SM, et al. Towards minimally-invasive, quantitative assessment of chronic kidney disease using optical spectroscopy. *Sci Rep.* 2019;9(1):7168.
34. Ravid JD, Kamel MH, and Chitalia VC. Uraemic solutes as therapeutic targets in CKD-associated cardiovascular disease. *Nature reviews Nephrology.* 2021.
35. von Maltzahn J, Chang NC, Bentzinger CF, and Rudnicki MA. Wnt signaling in myogenesis. *Trends in cell biology.* 2012;22(11):602-9.
36. Sato E, Mori T, Mishima E, Suzuki A, Sugawara S, Kurasawa N, et al. Metabolic alterations by indoxyl sulfate in skeletal muscle induce uremic sarcopenia in chronic kidney disease. *Sci Rep.* 2016;6:36618.

37. Chen J, Mohler ER, 3rd, Xie D, Shlipak MG, Townsend RR, Appel LJ, et al. Risk factors for peripheral arterial disease among patients with chronic kidney disease. *Am J Cardiol.* 2012;110(1):136-41.
38. Safe S, Cheng Y, and Jin UH. The Aryl Hydrocarbon Receptor (AhR) as a Drug Target for Cancer Chemotherapy. *Curr Opin Toxicol.* 2017;2:24-9.

Figure 1

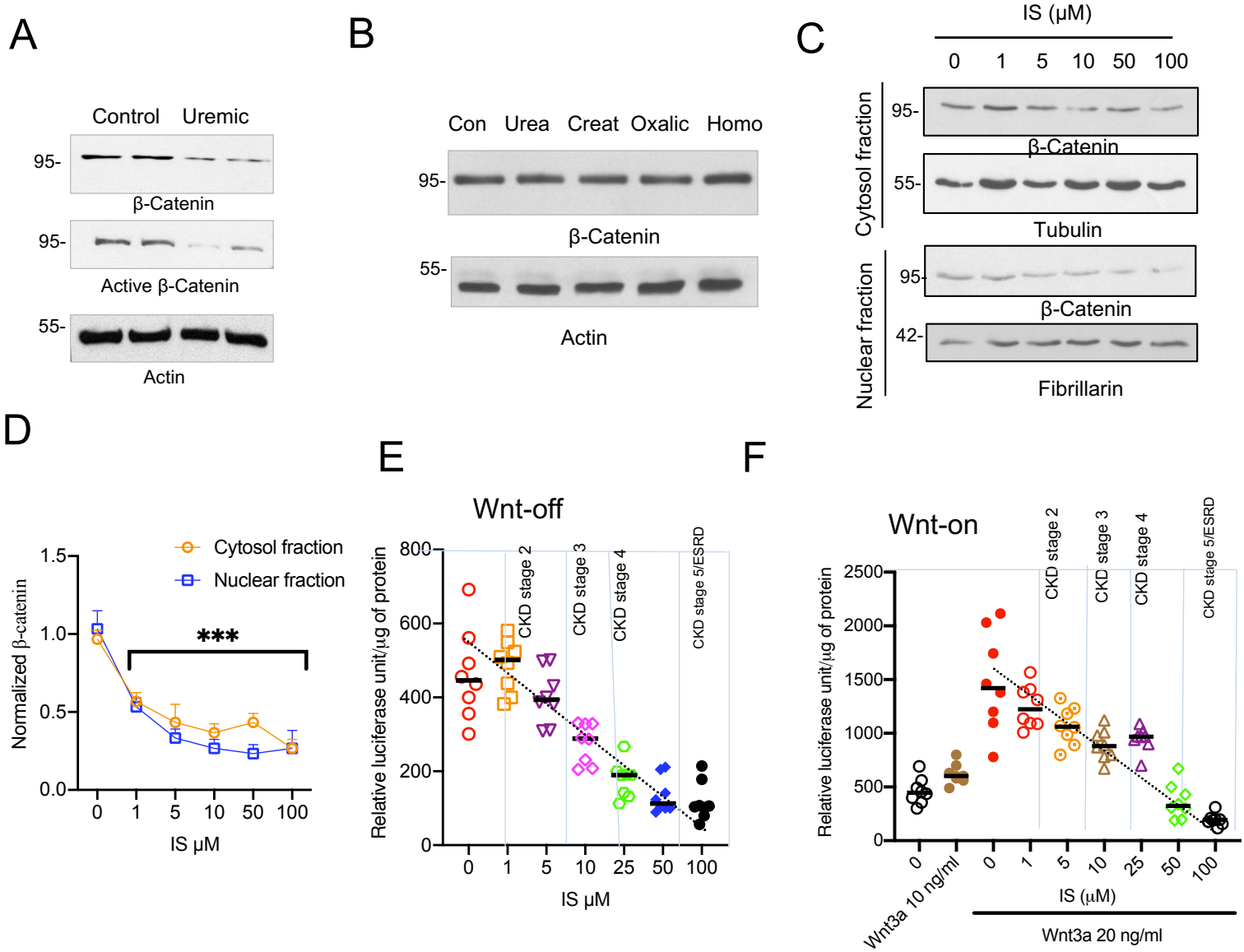
A
Control
Uremic
95-
β-Catenin
95-
Active β-Catenin
55-
Actin
B
Con
Urea
Creat
Oxalic
Homo
95-
β-Catenin
55-
Actin
C
IS (μM)
0
1
5
10
50
100
Cytosol fraction
95-
β-Catenin
55-
Tubulin
Nuclear fraction
95-
β-Catenin
42-
Fibrillarin
D
Cytosol fraction
Nuclear fraction
Normalized β-catenin
1.5
1.0
0.5
0.0
***
0
1
5
10
50
100
IS μM
E
Wnt-off
Relative luciferase unit/μg of protein
800
600
400
200
0
CKD stage 2
CKD stage 3
CKD stage 4
CKD stage 5/ESRD
0
1
5
10
25
50
100
IS μM
F
Wnt-on
Relative luciferase unit/μg of protein
2500
2000
1500
1000
500
0
CKD stage 2
CKD stage 3
CKD stage 4
CKD stage 5/ESRD
0
0
1
5
10
25
50
100
Wnt3a 10 ng/ml
IS (μM)
Wnt3a 20 ng/ml
G
Vehicle
Control
IS
Wnt 3a
Control
IS
Intensity
β-Catenin
DAPI
H
Normalized nuclear β-catenin
10
5
0
***
****
Control
IS
Control
IS
Vehicle
Wnt 3a

**Figure legends**

**Figure 1. Uremic serum and IS downregulate Wnt/β-catenin signaling in ECs.**

**(A).** Primary human microvascular endothelial cells (ECs) exposed to 5% pooled uremic or control sera. Equal amounts of protein were probed for β-catenin and separately for active β-catenin. Actin served as a loading control. Representative images from three independent experiments each done in duplicate are shown.

**(B).** Representative images of three independent experiments of ECs treated with water-soluble uremic toxins.

(**C**)**.** ECs pretreated with 5% of control serum and spiked with IS underwent fractionation. Tubulin and fibrillarin served as markers of fractions and loading controls. Representative images from four independent experiments.

**(D).** The β-catenin was normalized to loading controls for their fractions. Average of four independent experiments is shown. Error bars = SD. The cytosol and nuclear fractions were analyzed separately and compared to the control (IS = 0 μM) using Student's t-test with Bonferroni's correction of multiple comparisons.

(**E**). Serum-starved ECs expressing LS were treated with IS-spiked control human serum. Scatter plot of luciferase activity from two independent experiments done in quadruplet is shown. The horizontal line in each group corresponds to median. The blue dotted line corresponds to IS levels in different CKD stages (Table S2). A linear regression was performed.

(**F**). A luciferase activity assay was performed as above in ECs treated with Wnt3a and IS spiked-control human sera. Scatter plot of two independent experiments done in quadruplet is shown. A linear regression was performed.

(**G**). Serum starved ECs pre-treated with vehicle (PBS + 1% BSA) or Wnt 3a (20 ng/mL medium) with IS (50 μM) were stained. Representative images of 100 ECs/group. Profile plots were generated. Note different Y-axis scales between IS-treated and control samples. Scale bar = 5 micron.

**(H).** Fifty ECs/group were analyzed. The dot plot represents the integrated density of nuclear β-catenin normalized to the surface area of nucleus. The line corresponds to the median. Independent Student's t-tests were performed to compare the groups.

# Figure 2

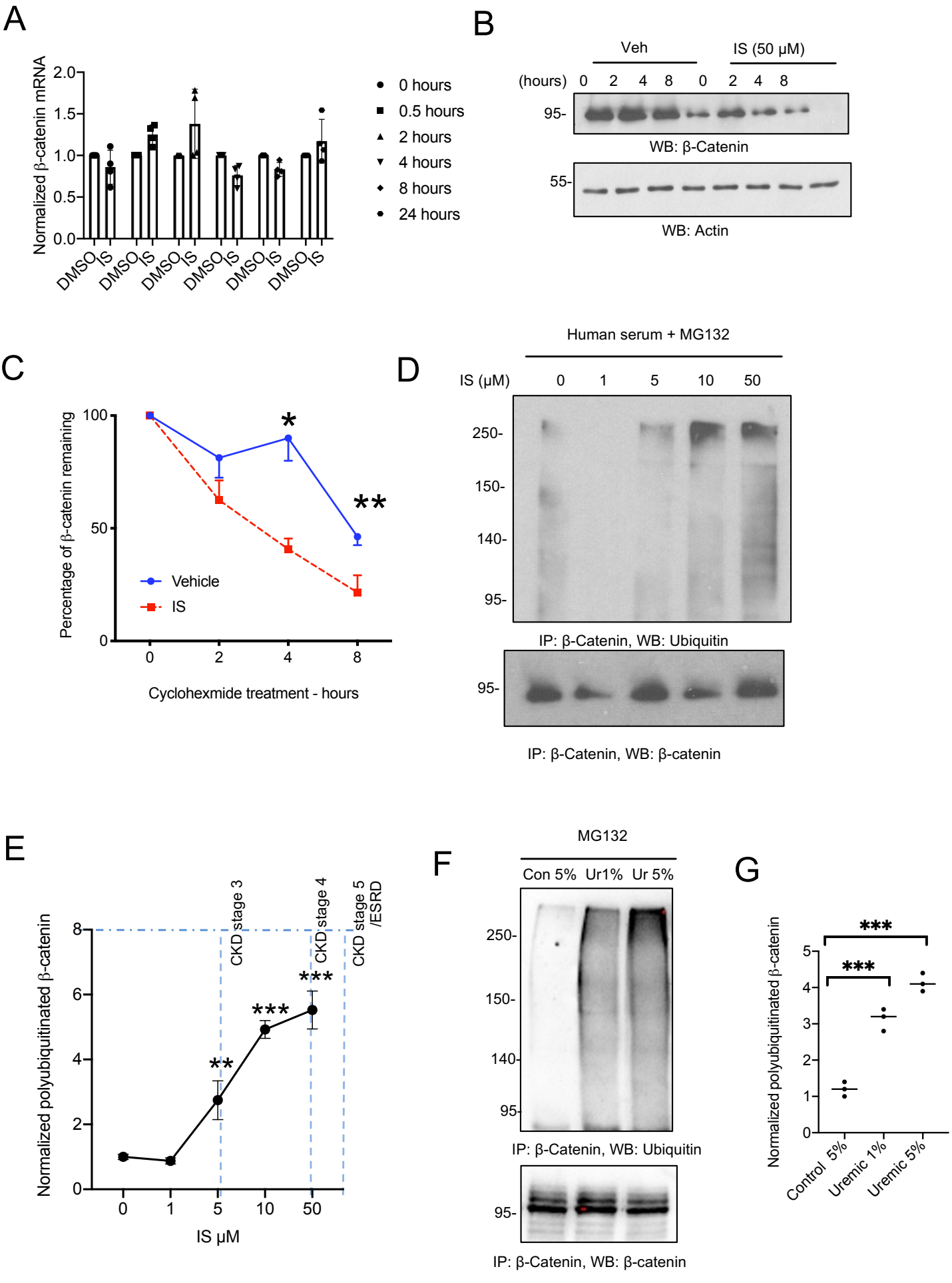
A
Normalized β-catenin mRNA
2.0
1.5
1.0
0.5
0.0
DMSO IS DMSO IS DMSO IS DMSO IS DMSO IS DMSO IS
0 hours
0.5 hours
2 hours
4 hours
8 hours
24 hours
B
Veh
IS (50 μM)
(hours) 0 2 4 8 0 2 4 8
95-
WB: β-Catenin
55-
WB: Actin
C
Percentage of β-catenin remaining
100
50
0
*
**
Vehicle
IS
0 2 4 8
Cyclohexmide treatment - hours
D
Human serum + MG132
IS (μM) 0 1 5 10 50
250-
150-
140-
95-
IP: β-Catenin, WB: Ubiquitin
95-
IP: β-Catenin, WB: β-catenin
E
Normalized polyubiquitinated β-catenin
8
6
4
2
0
CKD stage 3
CKD stage 4
CKD stage 5 /ESRD
**
***
***
0 1 5 10 50
IS μM
F
MG132
Con 5% Ur1% Ur 5%
250-
150-
140-
95-
IP: β-Catenin, WB: Ubiquitin
95-
IP: β-Catenin, WB: β-catenin
G
Normalized polyubiquitinated β-catenin
5
4
3
2
1
0
***
***
Control 5%
Uremic 1%
Uremic 5%

**Figure 2. IS augments polyubiquitination and degradation of β-catenin in ECs.**

**(A).** A qRT-PCR analysis of ECs treated with IS 50 μM or DMSO (control) for different times was performed. The average cycle threshold (Ct) values performed in triplicates are shown. Error bars = SD.

(**B**). ECs were treated with IS or vehicle (DMSO) for 24 hours and cycloheximide (30 μg/mL) for the indicated time. Representative images of four independent experiments are shown.

**(C).** β-catenin was normalized to actin and represented as the percentage of remaining β-catenin at each time point. Average of normalized β-catenin from four independent experiments is shown. Error bars = SD. Independent Student's t-tests were performed. Compared to vehicle-treated cells, IS treatment at each time point *p = 0.03 and **p = 0.001.

**(D).** ECs pretreated with 5% control human serum and spiked with IS corresponding to the different human CKD stages. The cells were exposed to MG132 10 μM overnight. Immunoprecipitation was performed. The blot was reprobed with anti-β-catenin antibody. Representative images of three independent experiments are shown.

**(E**). The ubiquitinated β-catenin was normalized to the immunoprecipitated β-catenin. Average of normalized ubiquitinated β-catenin from three experiments is shown. Student's t-test with Bonferroni correction was performed for multiple comparisons. Error bars = SD. Compared to vehicle-treated cells, **p = 0.01 and *** p <0.001. The blue dotted lines show IS levels corresponding to different CKD stages (Table S2).

**(F).** ECs pretreated with pooled control or uremic sera were processed as above. The blot was reprobed for β-catenin. Representative images of three independent experiments are shown.

(**G**). Average of normalized ubiquitinated β-catenin from three experiments is shown. Independent Student's t-tests were performed. Error bars = SD. *** p <0.001.

Figure 3

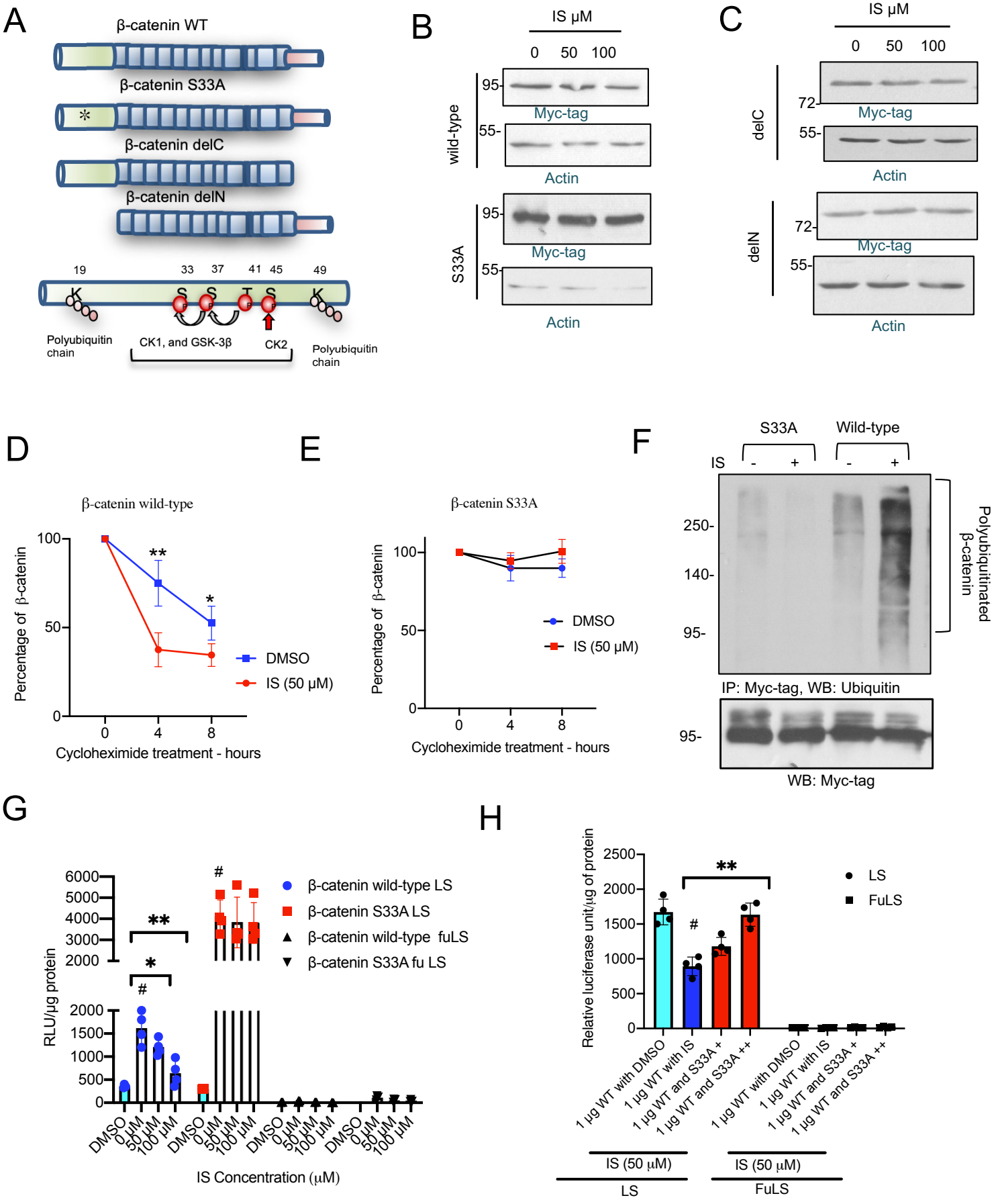
A
β-catenin WT
β-catenin S33A
β-catenin delC
β-catenin delN
19
33
37
41
45
49
Polyubiquitin chain
CK1, and GSK-3β
CK2
Polyubiquitin chain
B
IS μM
0 50 100
wild-type
95-
Myc-tag
55-
Actin
S33A
95-
Myc-tag
55-
Actin
C
IS μM
0 50 100
delC
72-
Myc-tag
55-
Actin
delN
72-
Myc-tag
55-
Actin
D
β-catenin wild-type
Percentage of β-catenin
100
50
0
**
*
DMSO
IS (50 μM)
0 4 8
Cycloheximide treatment - hours
E
β-catenin S33A
Percentage of β-catenin
100
50
0
DMSO
IS (50 μM)
0 4 8
Cycloheximide treatment - hours
F
S33A
Wild-type
IS
- + - +
250-
140-
95-
Polyubiquitinated β-catenin
IP: Myc-tag, WB: Ubiquitin
95-
WB: Myc-tag
G
RLU/μg protein
6000
5000
4000
3000
2000
**
*
#
#
β-catenin wild-type LS
β-catenin S33A LS
β-catenin wild-type fuLS
β-catenin S33A fu LS
2000
1500
1000
500
0
DMSO 0 μM 50 μM 100 μM
IS Concentration (μM)
H
Relative luciferase unit/μg of protein
2500
2000
1500
1000
500
0
**
#
LS
FuLS
1 μg WT with DMSO
1 μg WT with IS
1 μg WT and S33A +
1 μg WT and S33A ++
IS (50 μM)
LS
IS (50 μM)
FuLS

**Figure 3. IS downregulates β-catenin dependent on S33 residue in the degron motif.**

**(A)**. β-catenin N terminus contains a degron motif which controls its degradation. A black asterisk marks β-catenin S33A. Myc-tagged truncations lack N- terminus (delN) and C-terminus (delC).

**(B)**. ECs pre-transfected with Myc-tagged β-catenin wild-type or S33A were treated with IS. Representative images of three independent experiments.

(**C**). ECs pre-transfected with Myc-tagged delC or delN β-catenin were treated with IS. Representative images of three independent experiments.

**(D)**. ECs transfected with wild-type β-catenin were treated with IS (50 μM) and cycloheximide (30 μg/mL) for indicated time. Average of normalized β-catenin from four independent experiments is shown. Error bars = SD. Independent Student's t-tests were performed at different time points. **p = 0.01 and *p = 0.04.

(**E**). Half-life study of Myc-tagged β-catenin S33A was performed as above from four independent experiments. Error bars = SD.

**(F)**. ECs pre-transfected with Myc-tag β-catenin wild-type or S33A were treated with IS 50 μM and MG132 10 μM before harvest. Immunoprecipitation was performed. The lysates were probed separately with anti-Myc-tag antibody. Representative images of three independent experiments are shown.

(**G**). ECs stably expressing LS and Fu LS constructs were co-transfected with Myc-tagged wild-type or S33A β-catenin and were treated with IS or DMSO followed by a luciferase assay. Average of three experiments done in triplicate is shown. Error bars = SD. Independent Student's t-tests were performed.

(**H**). ECs stably expressing LS and FuLS constructs were co-transfected with Myc-tagged wild-type (WT) and increasing amounts of S33A β-catenin (shown as + and ++ marks). Expression of

β-catenin wild-type or S33A was confirmed (**Figure S5E**). Average of three experiments done in triplicate is shown. Error bars = SD. Independent Student's t-tests were performed.

# Figure 4

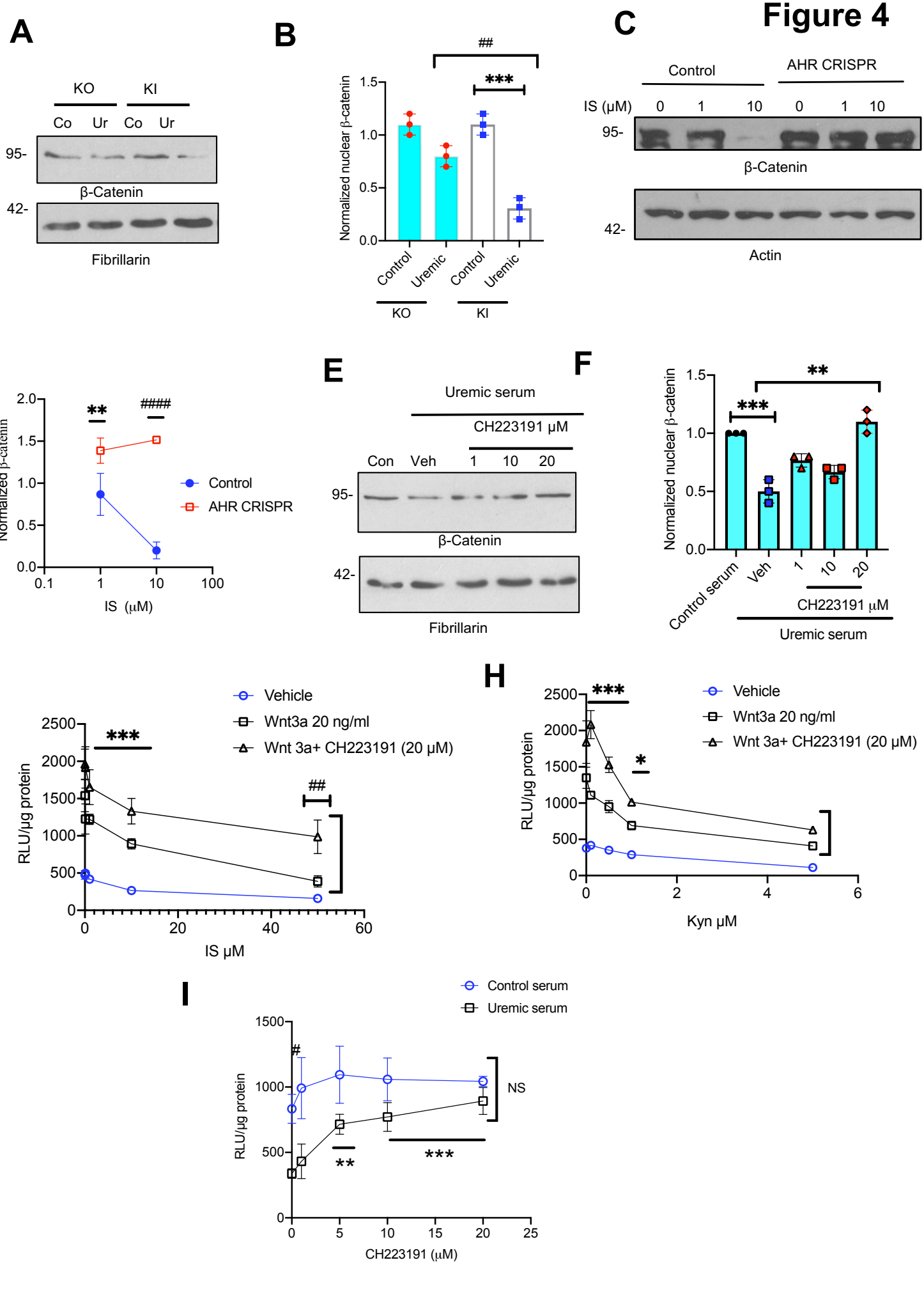
A
KO
KI
Co
Ur
Co
Ur
95-
β-Catenin
42-
Fibrillarin
B
##
***
Normalized nuclear β-catenin
1.5
1.0
0.5
0.0
Control
Uremic
Control
Uremic
KO
KI
C
Control
AHR CRISPR
IS (μM)
0
1
10
0
1
10
95-
β-Catenin
42-
Actin
D
**
####
Normalized β-catenin
2.0
1.5
1.0
0.5
0.0
0.1
1
10
100
IS (μM)
Control
AHR CRISPR
E
Uremic serum
CH223191 μM
Con
Veh
1
10
20
95-
β-Catenin
42-
Fibrillarin
F
**
***
Normalized nuclear β-catenin
1.5
1.0
0.5
0.0
Control serum
Veh
1
10
20
CH223191 μM
Uremic serum
G
Vehicle
Wnt3a 20 ng/ml
Wnt 3a+ CH223191 (20 μM)
***
##
RLU/μg protein
2500
2000
1500
1000
500
0
0
20
40
60
IS μM
H
Vehicle
Wnt3a 20 ng/ml
Wnt 3a+ CH223191 (20 μM)
***
*
RLU/μg protein
2500
2000
1500
1000
500
0
0
2
4
6
Kyn μM
I
Control serum
Uremic serum
#
**
***
NS
RLU/μg protein
1500
1000
500
0
0
5
10
15
20
25
CH223191 (μM)

**Figure 4. Uremic serum and uremic solutes mediate Wnt/β-catenin suppressive effect through AHR signaling.**

**(A**). AHR KI and KO MEFs treated with pooled 5% control or uremic sera. Their nuclear fractions were probed. Representative images of three independent experiments are shown.

(**B**). Average of normalized nuclear β-catenin from three experiments is shown. Independent Student's t-tests were performed. Error bars = SD.

(**C**). The ECs knocked out of AHR (AHR CRISPR) were treated with IS. Representative images of three independent experiments are shown.

(**D**). Average of normalized β-catenin from three independent experiments. Scale bar= SEM. Student's t-test was performed.

(**E**). Representative images of the nuclear fractions of ECs treated with 5% pooled uremic serum with CH223191 from three independent experiments are shown.

(**F**). Average of normalized β-catenin from three experiments is shown. Student's t-test with Bonferroni correction was performed for multiple comparisons. Error bars = SD.

(**G-I**). ECs expressing LS were treated with IS and Wnt3a 20 ng/mL with or without 20 μM CH223191 (**G**), with Kyn and Wnt3a 20 ng/mL with or without 20 μM CH223191 (**H**), with 5% pooled control or uremic serum with CH223191 (**I**). Averages for six independent repeats in each figure are shown. Error bars = SEM. ANOVA test was performed to compare groups ($p < 0.001$). The pairwise comparisons with Tukey's multiple comparison procedure were performed.

Figure 5

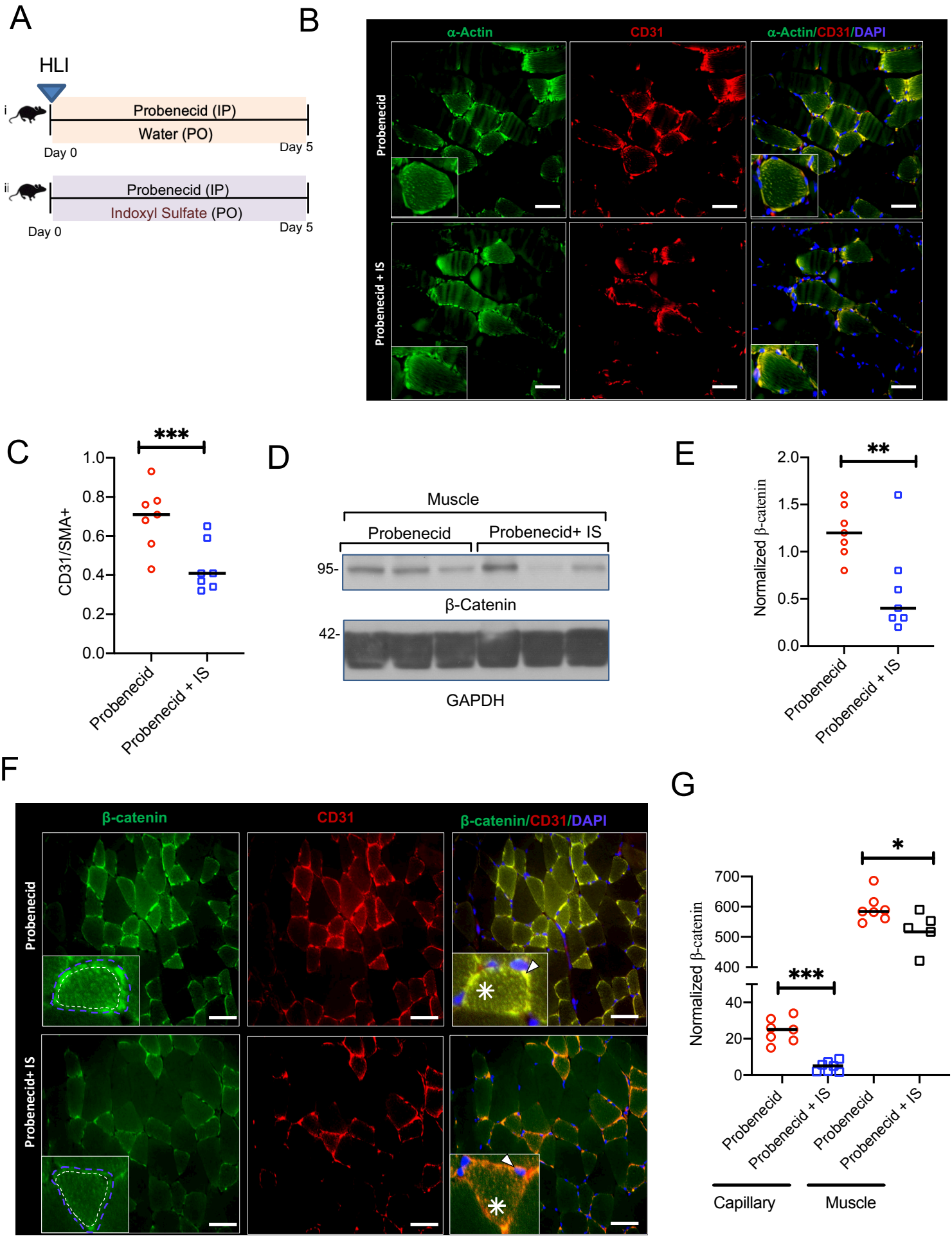
A
HLI
i
Probenecid (IP)
Water (PO)
Day 0
Day 5
ii
Probenecid (IP)
Indoxyl Sulfate (PO)
Day 0
Day 5
B
α-Actin
CD31
α-Actin/CD31/DAPI
Probenecid
Probenecid + IS
C
***
CD31/SMA+
1.0
0.8
0.6
0.4
0.2
0.0
Probenecid
Probenecid + IS
D
Muscle
Probenecid
Probenecid+ IS
95-
β-Catenin
42-
GAPDH
E
**
Normalized β-catenin
2.0
1.5
1.0
0.5
0.0
Probenecid
Probenecid + IS
F
β-catenin
CD31
β-catenin/CD31/DAPI
Probenecid
Probenecid+ IS
G
*
***
Normalized β-catenin
700
600
500
400
40
20
0
Probenecid
Probenecid + IS
Probenecid
Probenecid + IS
Capillary
Muscle

**Figure 5. IS suppressed post-ischemic angiogenesis and β-catenin expression in mice.**

(**A**). A group of 8-12 weeks old C57BL/6 female mice were initiated on Probenecid (N= 7) or Probenecid + IS (N= 7) and underwent HLI followed by harvest after 5 days.

(**B**). Representative images of the posterior calf muscles from the ligated limbs of mice stained for α-actin and CD31. A total of 30 images per group (N=7 mice/group). The inserts show myocyte with surrounding capillaries. Scale bar = 25 micron

(**C**). The integrated density of CD31+ was normalized to that of α-actin and presented as a ratio. A total of thirty images from 7 mice/group are shown and the line represents the median. Student's t-test was performed. **p = 0.001.

**(D).** The lysates of posterior calf muscles of the ligated limb of mice were probed. Representative immunoblots from three separate mice from each group of (N = 7 mice/group).

(**E**)**.** Normalized β-catenin in muscle lysates is presented in box-and-whisker plot. Student's t-test was performed. **p = 0.007.

(**F**). Four to five random images of posterior calf muscles from the ligated limbs of mice were stained for β-catenin and CD31. The inserts show a myocyte with β-catenin with surrounding capillaries. The blue dotted line represents ROI of a muscle surrounded by capillaries; and the white dotted line represents the ROI of a muscle. The white asterisk corresponds to β-catenin in a muscle. White arrowhead is directed to β-catenin in the capillary. Scale bar = 25 micron

(**G**). First, the integrated density was estimated from the ROI of the blue dotted line (β-catenin in a muscle with surrounding capillary). Next, the integrated density was analyzed only from the white dotted line (β-catenin in muscles). Their differences correspond to β-catenin in the capillaries. The integrated densities of capillaries and muscles from thirty random images (N=7

mice/group) are shown. The line represents the median. Student's t-test was performed. **** $p < 0.001$ and * $p < 0.05$.

Figure 6

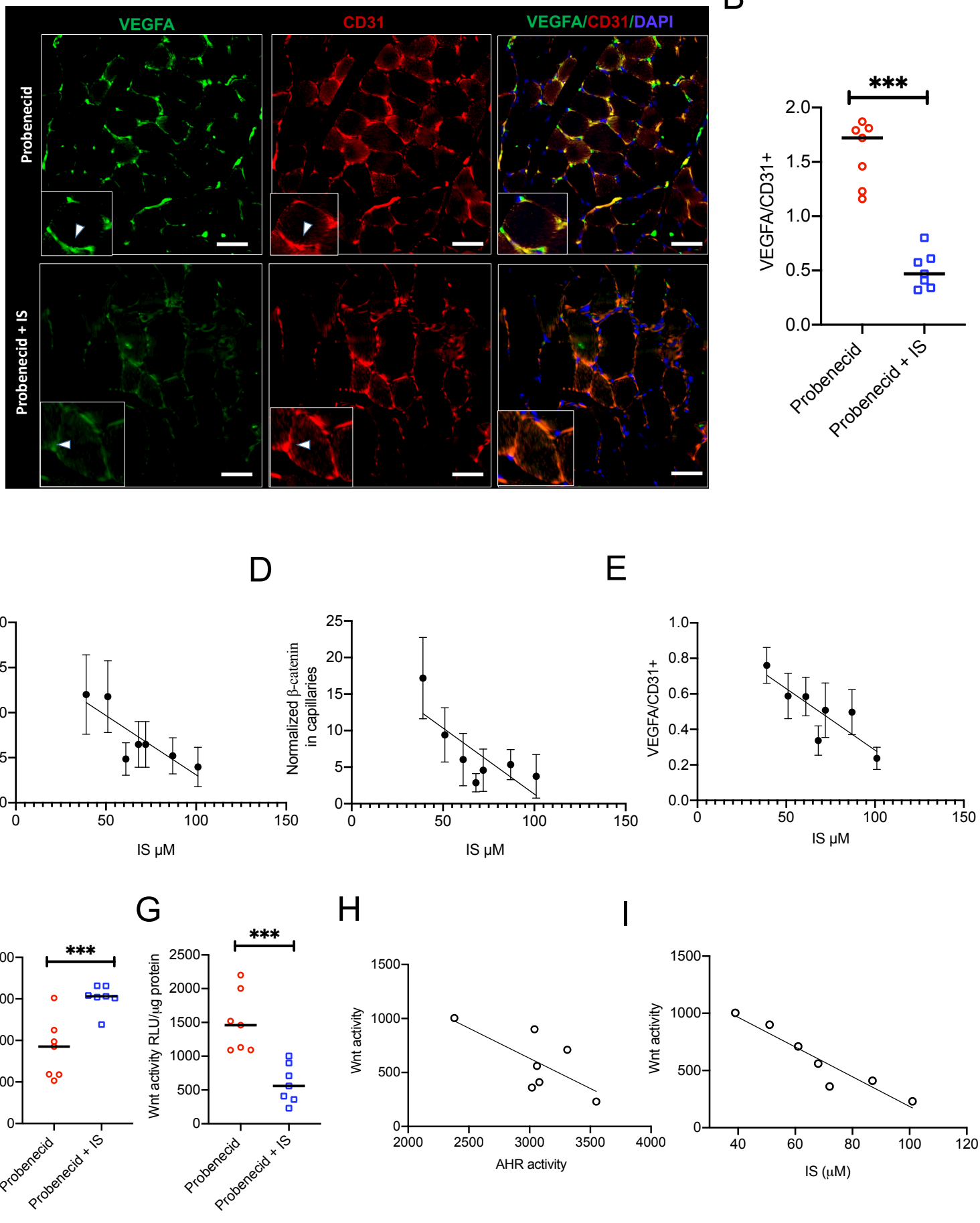
A
VEGFA
CD31
VEGFA/CD31/DAPI
Probenecid
Probenecid + IS
B
***
VEGFA/CD31+
2.0
1.5
1.0
0.5
0.0
Probenecid
Probenecid + IS
C
CD31/SMA+
2.0
1.5
1.0
0.5
0.0
0
50
100
150
IS μM
D
Normalized β-catenin in capillaries
25
20
15
10
5
0
0
50
100
150
IS μM
E
VEGFA/CD31+
1.0
0.8
0.6
0.4
0.2
0.0
0
50
100
150
IS μM
F
***
AHR RLU/μg protein
4000
3000
2000
1000
0
Probenecid
Probenecid + IS
G
***
Wnt activity RLU/μg protein
2500
2000
1500
1000
500
0
Probenecid
Probenecid + IS
H
Wnt activity
1500
1000
500
0
2000
2500
3000
3500
4000
AHR activity
I
Wnt activity
1500
1000
500
0
40
60
80
100
120
IS (μM)

**Figure 6. IS-specific solute mouse model shows suppressed VEGF-A expression and angiogenic phenotype in an IS- and AHR-dependent manner.**

(**A**) Representative images from thirty random images (N= 7 mice/group) of the posterior calf muscles from the ligated limbs were stained. The inserts show a representative myocyte with surrounding capillaries. The white arrowhead corresponds to VEGF or CD31. Scale bar = 25 micron.

(**B**) The integrated density of VEGF-A and CD31 were estimated from thirty images from each group (N= 7 mice/group). The line represents the median. Student's t-test was performed. *** p = 0.001.

(**C-E**). Correlations between IS levels and capillary density (CD31/SMA+) (**J**) and normalized β-catenin in capillaries (**K**) and normalized VEGF-A in the ischemic limb of IS-exposed mice (N= 7) (**L**).

(**F-G**). ECs expressing XRE-responsive promoter (**M**) or LS (N) treated with sera from mice from two groups (N= 7/group). Line corresponds to median. Student's t-test was performed.

**(H-I)** Correlation between ECs Wnt and AHR activity in response to sera from IS-exposed mice **(H);** and IS levels and EC Wnt activity in response to sera from these mice N = 7 (**I**).

Figure 7

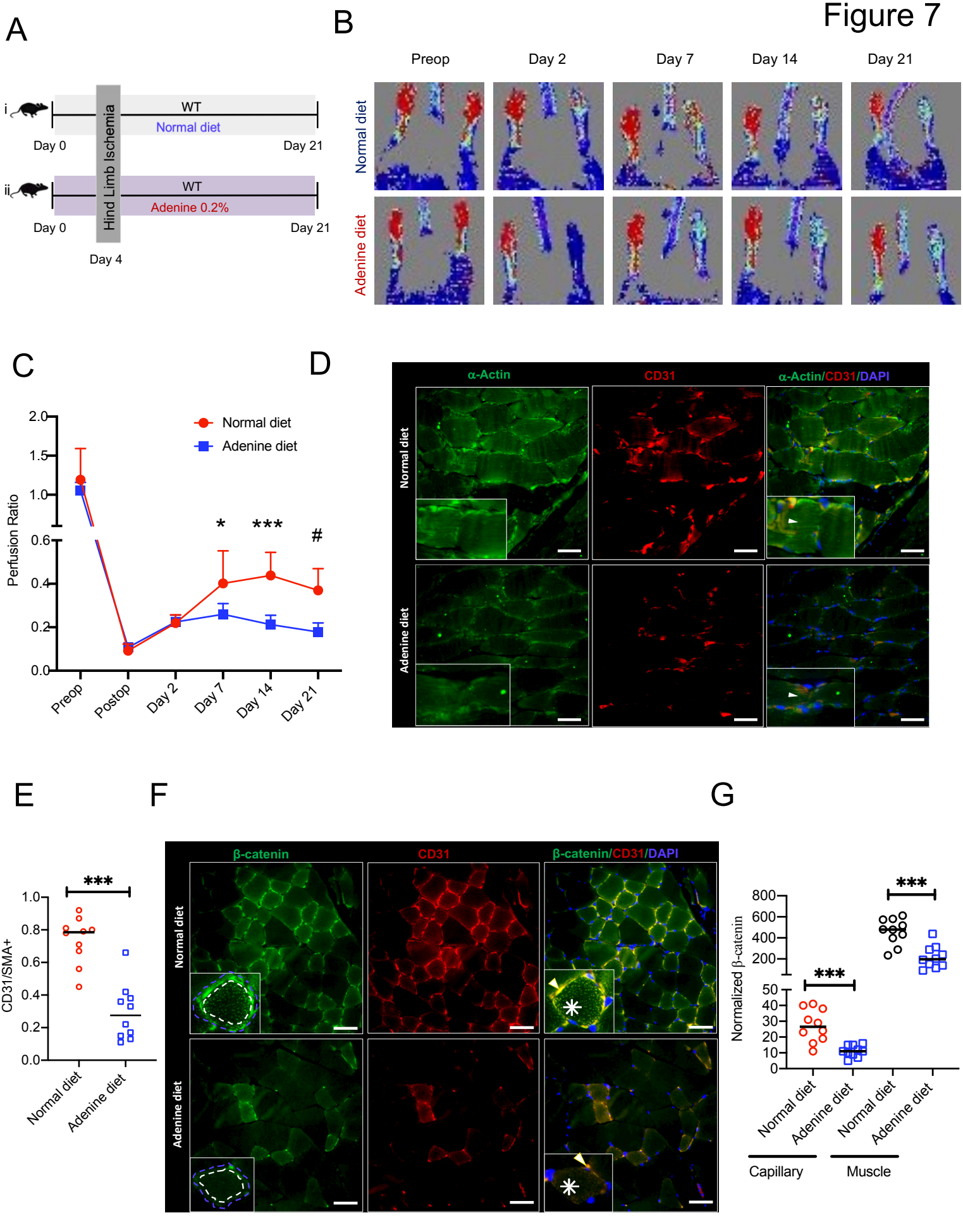
A
i
WT
Normal diet
Day 0
Day 21
Hind Limb Ischemia
ii
WT
Adenine 0.2%
Day 0
Day 21
Day 4
B
Preop
Day 2
Day 7
Day 14
Day 21
Normal diet
Adenine diet
C
Normal diet
Adenine diet
Perfusion Ratio
2.0
1.5
1.0
0.6
0.4
0.2
0.0
*
***
#
Preop
Postop
Day 2
Day 7
Day 14
Day 21
D
α-Actin
CD31
α-Actin/CD31/DAPI
Normal diet
Adenine diet
E
CD31/SMA+
1.0
0.8
0.6
0.4
0.2
0.0
***
Normal diet
Adenine diet
F
β-catenin
CD31
β-catenin/CD31/DAPI
Normal diet
Adenine diet
G
Normalized β-catenin
800
600
400
200
50
40
30
20
10
0
***
***
Normal diet
Adenine diet
Normal diet
Adenine diet
Capillary
Muscle

**Figure 7. Adenine-induced CKD model shows compromised angiogenesis and β-catenin expression in the ligated limb of mice.**

**(A).** A group of 8- to 12-week-old C57BL/6 female mice on a 0.2% adenine diet (N= 10) or the control diet (N= 10) underwent HLI and harvested at the end of 21 days.

**(B).** Representative laser doppler images of mice hind paws N= 10 mice/per group.

**(C).** Average perfusion ratios. Error bars = SD. Independent Student's t-tests were applied to compare two groups at each time point.

**(D).** Three random images from stained posterior calf muscles of the ligated limbs of each mouse (N= 10 mice/group). The insert represents a myocyte, where a white arrowhead is directed at α-Actin expression. Scale bar = 25 micron.

(**E**). An average of the normalized integrated density of CD3 to α-Actin per image described in Figure 6D are shown. The line represents median. Student's t-test was performed. *** $p < 0.001$.

(**F**) Three random images of stained posterior calf muscles of the ligated limb per mouse (N= 10 mice/group). The inserts show a myocyte stained with β-catenin with surrounding capillaries. The blue dotted line represents ROI of a myocyte and capillaries; and the white dotted line represents ROI of a myocyte. The white asterisk corresponds to β-catenin in a myocyte. White arrowhead is directed to β-catenin in a capillary. Scale bar = 25 micron

(**G**). The normalized integrated densities of β-catenin of muscles and capillaries obtained from thirty random images per group (N = 10 mice/group). The line represents median. Student's t-test was performed. **** $p < 0.001$ and ** $p = 0.001$.

Figure 8

A

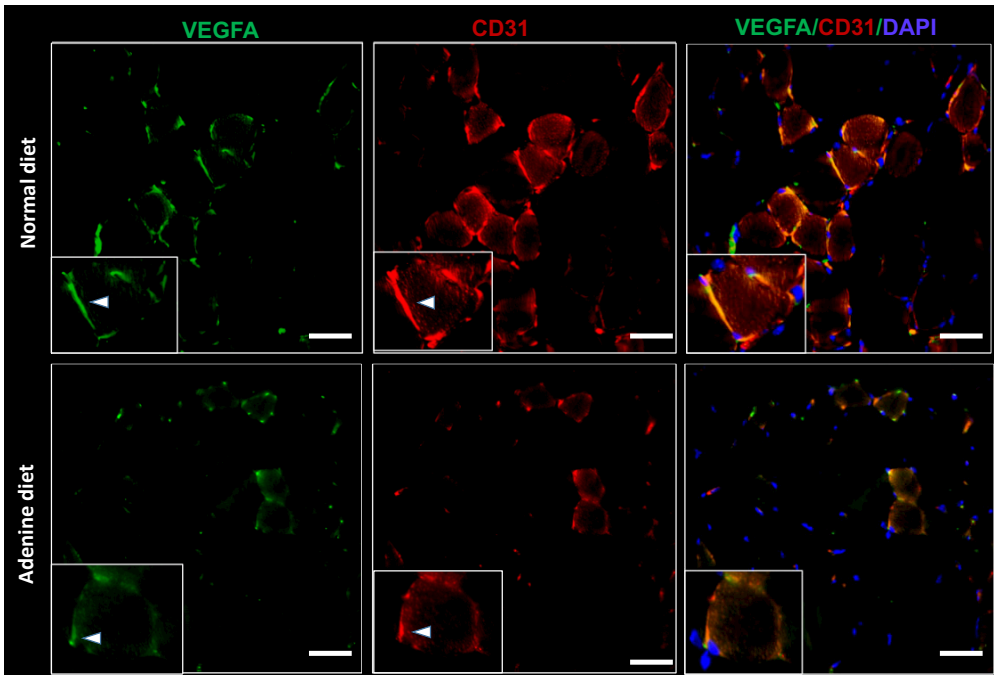


B

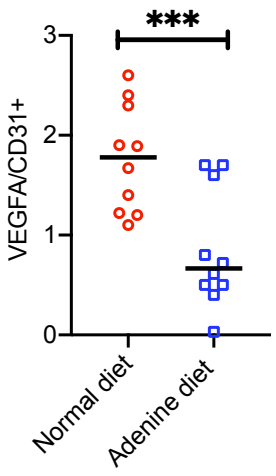


C

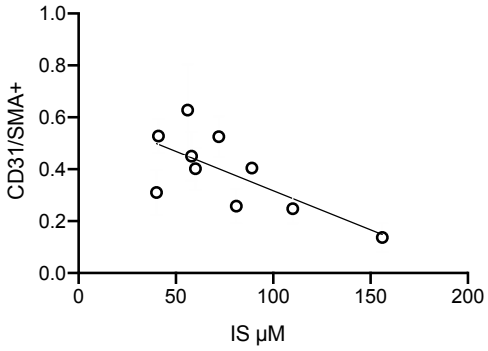


D

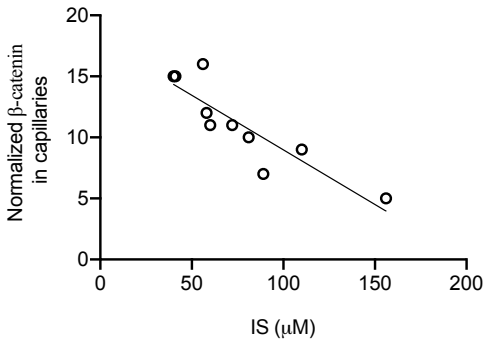


E

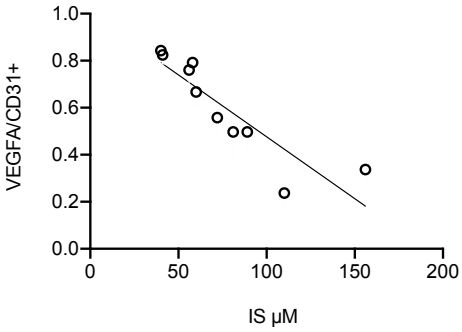


F

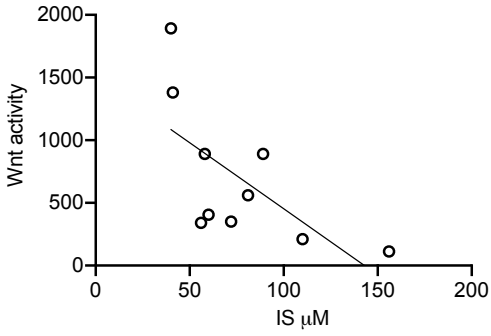


G

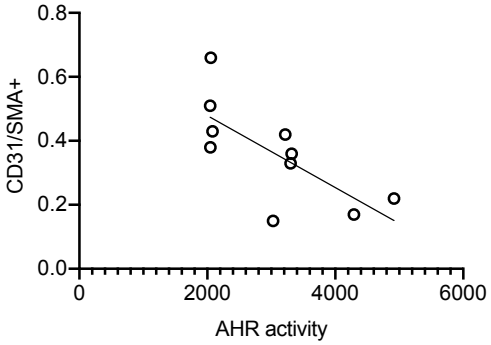

**Figure 8. Adenine-induced CKD model shows suppressed VEGF-A and angiogenic response in an IS- and AHR-dependent manner.**

(**A**) Representative images from three randomly taken images per mouse (N= 10 mice/group). The inserts show a representative myocyte with a white arrowhead directed to VEGF or CD31. Scale bar = 25 micron.

(**B**) The integrated densities of normalized VEGF-A from images obtained from Figure 6H. The line represents median. Student's t-test was performed. *** p = 0.003.

(**C-E**). Correlations between the IS levels and histological parameter in the ischemic limb of CKD mice (N= 10).

**(F-G)** Correlations between EC Wnt activity in response to sera from CKD mice and their IS levels **(F)** and the capillary density in CKD mice and AHR activity in ECs in response to sera from these mice N = 10 (**G**).

Figure 9

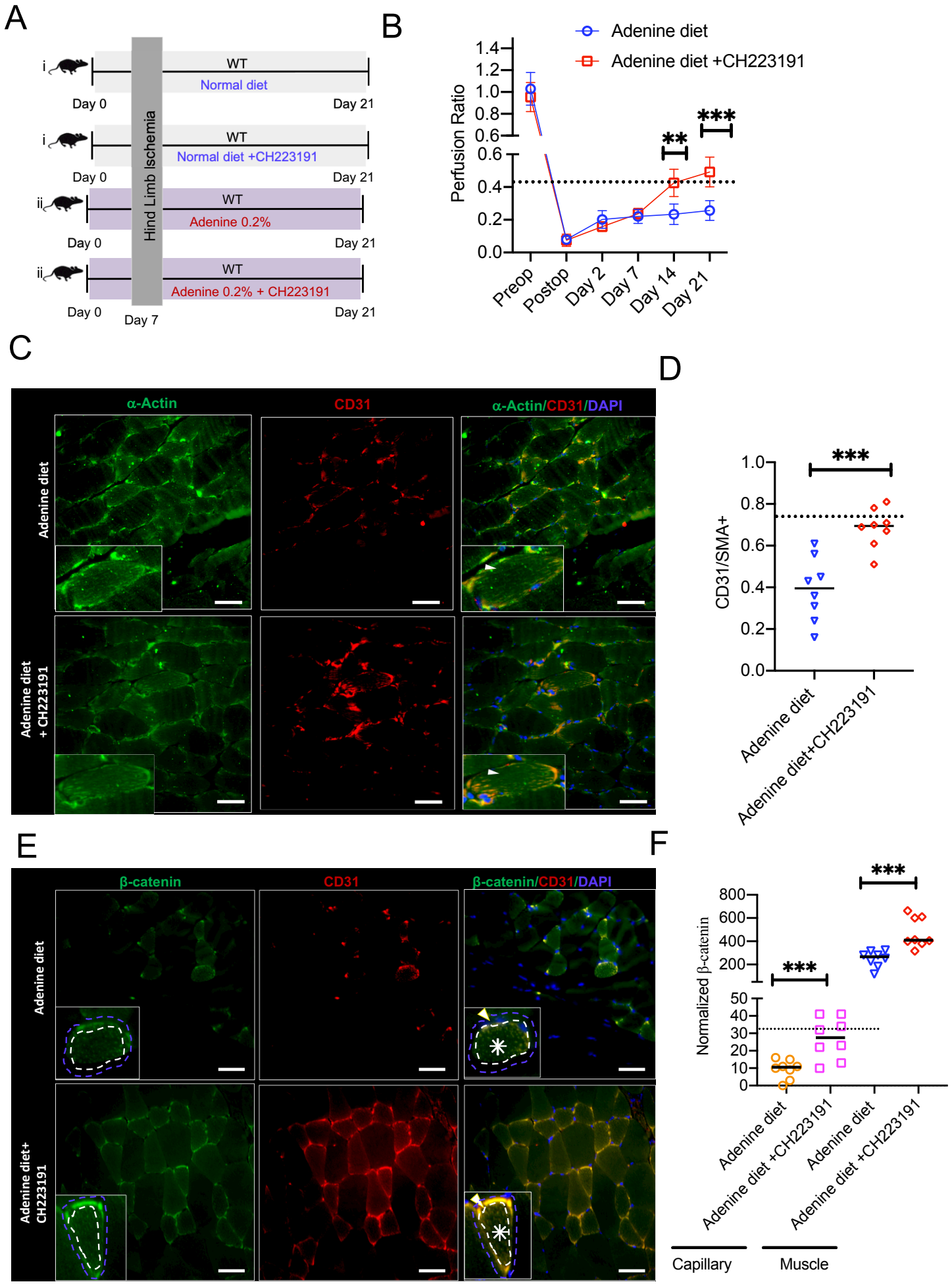
A
i
WT
Normal diet
Day 0
Day 21
i
WT
Normal diet +CH223191
Day 0
Day 21
ii
WT
Adenine 0.2%
Day 0
Day 21
ii
WT
Adenine 0.2% + CH223191
Day 0
Day 7
Day 21
Hind Limb Ischemia
B
Adenine diet
Adenine diet +CH223191
Perfusion Ratio
1.4
1.2
1.0
0.8
0.6
0.6
0.4
0.2
0.0
**
***
Preop
Postop
Day 2
Day 7
Day 14
Day 21
C
α-Actin
CD31
α-Actin/CD31/DAPI
Adenine diet
Adenine diet + CH223191
D
CD31/SMA+
1.0
0.8
0.6
0.4
0.2
0.0
***
Adenine diet
Adenine diet+CH223191
E
β-catenin
CD31
β-catenin/CD31/DAPI
Adenine diet
Adenine diet+ CH223191
F
Normalized β-catenin
800
600
400
200
50
40
30
20
10
0
***
***
Adenine diet
Adenine diet +CH223191
Adenine diet
Adenine diet +CH223191
Capillary
Muscle

**Figure 9. AHR inhibition normalizes post-ischemic angiogenesis in CKD mice to a non-CKD level.**

**(A).** A group of C57BL/6 female mice on a 0.2% adenine diet (N= 16) or the control diet (N= 16) for 7 days underwent HLI. The mice were randomized to two groups, N= 8/group and initiated on DMSO or CH223191 for 5 days and 2 days off for two weeks.

**(B).** Average perfusion ratios N= 8 mice/group. Error bars = SD. Independent Student's t-tests were applied at each time point. The dotted line in this graph and subsequent figures corresponds to the respective values of mice on normal diet.

**(C).** Representative stained images from three random images per mouse (N=8 mice/group) of the posterior calf muscles from ligated limbs of mice. The insert represents a myocyte. The white arrowhead is directed at α-Actin expression. Scale bar = 25 micron.

**(D).** Integrated density of CD31 normalized to α-Actin described in Figure 7C. The line represents median value. Student's t-test was performed. *** $p < 0.001$.

**(E).** Representative stained images from three random images per mouse (N=8 mice/group) of the posterior calf muscles from ligated limbs of mice. The inserts show a representative myocyte stained with β-catenin along with surrounding capillaries. The blue dotted line is the ROI of a myocyte and capillaries; and the white dotted line is the ROI of a myocyte. The white asterisk corresponds to β-catenin in a myocyte. White arrowhead is directed to β-catenin in the capillary. Scale bar = 25 micron.

**(F).** The integrated densities of normalized β-catenin in muscles and capillaries from eight mice per group. The line represents median. Student's t-test was performed. *** $p = 0.002$ and *** $p < 0.001$.

# Figure 10

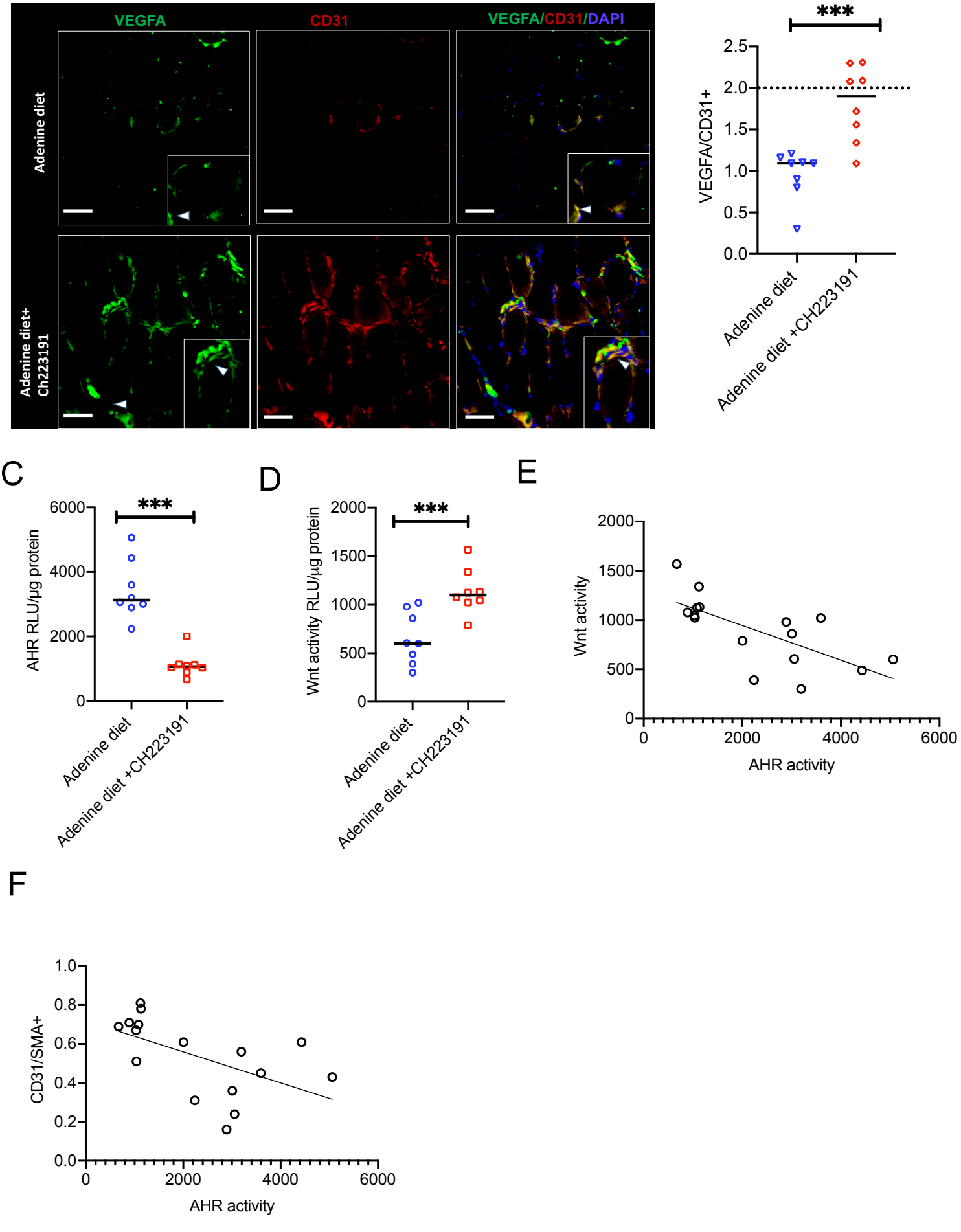
A
VEGFA
CD31
VEGFA/CD31/DAPI
Adenine diet
Adenine diet+ Ch223191
B
***
VEGFA/CD31+
2.5
2.0
1.5
1.0
0.5
0.0
Adenine diet
Adenine diet +CH223191
C
***
AHR RLU/µg protein
6000
4000
2000
0
Adenine diet
Adenine diet +CH223191
D
***
Wnt activity RLU/µg protein
2000
1500
1000
500
0
Adenine diet
Adenine diet +CH223191
E
Wnt activity
2000
1500
1000
500
0
0
2000
4000
6000
AHR activity
F
CD31/SMA+
1.0
0.8
0.6
0.4
0.2
0.0
0
2000
4000
6000
AHR activity

**Figure 10. AHR inhibition improves angiogenic response in CKD mice.**

**(A).** Representative images of the posterior calf muscles from ligated limbs of mice from three randomly images per mouse (N= 8 mice/group). The inserts show a myocyte with a white arrowhead directed to VEGF or CD31. Scale bar = 25 micron.

**(B)** The integrated density of normalized VEGF-A to CD31 from images in Figure 7G. The line represents median. Student's t-test was performed. *** $p < 0.001$.

**(C)** ECs expressing XRE-promoter-luciferase reporter were treated with 1% sera from mice from adenine-treated mice with or without CH223191. Average for six luciferase independent repeats is shown. Error bars = SEM. Student's t-test was performed. AHR activity *** $p < 0.001$.

**(D)** ECs expressing LS were treated with 1% sera from mice from both the groups. Average for six independent repeats of Wnt activity is shown. Error bars = SEM. Student's t-test was performed. ***$p < 0.001$.

**(E).** A correlation between AHR activity and Wnt activity in ECs in response to the sera from adenine-treated mice with or without CH223191.

(**F**). A correlation between the EC AHR activity in response to the sera from mice listed in panel K and their capillary density in muscles of ligated limb.

**Table 1. Patient characteristics of PAD cohort**

| **Parameters** | **No Adverse Limb Event N= 35** | **Adverse Limb Event N = 28** |
|---|---|---|
| Age, years | 70.1±11.8 | 65.4± 7.6 |
| Male | 17 | 15 |
| BMI, $kg/m^2$ | Mean: 29.7 ± 6.8 | Mean: 29.4 ± 6.5 |
| Black Race, % (N) | 34 (12) | 29 (8) |
| Diabetes Mellitus, % (N) | 51 (18) | 50 (14) |
| Coronary artery disease, % (N) | 65 (23) | 54 (15) |
| Smoking | 40 (14) | 36 (10) |
| Blood pressure, mm Hg | | |
| Systolic mm of Hg | 145 ± 24 | 143 ± 22 |
| Diastolic mm of Hg | 72 ± 9 | 71 ± 10 |
| eGFR ml/min/sq mt Body | 50 ± 27 | 64 ± 30 |
| Ankle-brachial index, mmHg | 0.62 ± 0.19 | 0.63 ± 0.25 |
| Data presented as Mean ± SD unless otherwise noted, all P=NS by t-test or chi-square | | |

**Table 2: Association of Uremic Solutes and AHR and Wnt activity in ECs with Adverse Limb Events**

| Parameter | HR | 95% CI | P value |
|---|---|---|---|
| IS (μM) | 2.2 | 1.3-3.7 | 0.003 |
| Kyn (nM) | 4.2 | 1.9-9.3 | 0.0003 |
| KA (nM) | 2.5 | 1.2-4.9 | 0.01 |
| AA (μM) | 0.95 | 0.61-1.4 | 0.78 |
| XA (μM) | 2.3 | 1.3-4.1 | 0.003 |
| QA (μM) | 1.9 | 0.63-2.5 | 0.65 |
| Trp (μM) | 1.6 | 0.63-3.7 | 0.11 |
| Wnt activity (RLU/μg protein)# | 0.52 | 0.27-0.97 | 0.04 |
| AHR activity (RLU//μg protein)# | 4.2 | 1.2-14.4 | 0.02 |

Adjusting for age, sex, GFR. All measures ln transformed for analysis
IS- indoxyl sulfate, Kyn – Kynurenine, KA – Kynurenic acid, AA – Anthranilic acid, XA- Xanthurenic acid, QA- Quinolinic acid, Trp – Tryptophan.
Assays examine the ability of plasma from PAD patients to induce Wnt and AHR activity in ECs.